activity. Although the reported role of CITED2 in hypoxic stress does not coincide with our present results [32], our present histopathological study supports a scenario in human UC involving another CITED2-activating pathway. Thus, highly concentrated BA produced by enteric bacteria would induce CITED2-p53-dependent apoptosis in the colonic epithelium and cause erosion, which is typical of active UC. With mucosal erosion, enteric bacteria can easily infiltrate into the colonic stroma and stimulate macrophages [41], which would enhance inflammation by producing inflammatory cytokines. Apoptosis induced by BA was here inhibited by an siRNA for p53, as well as by 4CHC, an inhibitor of MCT1 (Fig. 4b), which suggests the possibility of anti-inflammation targeted therapy. However, mechanisms of UC generation still need further analysis, particular with regard to enteric bacteria. In conclusion, we propose that p53 activation via CITED2 upregulation by BA and consequent p53 acetylation is a possible mechanism underlying UC development.

Acknowledgments The authors appreciate the technical assistance of Ms. Y. Numata and would like to thank Dr. M. Moore for revising the English of the manuscript. This work was supported in part by Grants-in-Aid for Scientific Research from the Japan Society for the Promotion of Science, Health Sciences Research Grants H18-Kagaku-Ippan-001 from the Ministry of Health, Labour and Welfare, Japan, Grants-in-Aid from Kitasato University Graduate School of Medical Sciences and Kanagawa Nanbyo Foundation.

Conflicts of interest The authors disclose no conflicts with this work.

References

1. Arai N, Mitomi H, Ohtani Y, Igarashi M, Kakita A, Okayasu I. Enhanced epithelial cell turnover associated with p53 accumulation and high p21WAF1/CIP1 expression in ulcerative colitis. Mod Pathol. 1999;12:604–11.
2. Mitsuhashi J, Mikami T, Saigenji K, Okayasu I. Significant correlation of morphological remodeling in ulcerative colitis with disease duration and between elevated p53 and p21 expression in rectal mucosa and neoplastic development. Pathol Int. 2005;55:113–21.
3. Okayasu I, Hatakeyama S, Yamada M, Ohkusa T, Inagaki Y, Nakaya R. A novel method in the induction of reliable experimental acute and chronic ulcerative colitis in mice. Gastroenterology. 1990;98:694–702.
4. Okayasu I, Ohkusa T, Kajiura K, Kanno J, Sakamoto S. Promotion of colorectal neoplasia in experimental murine ulcerative colitis. Gut. 1996;39:87–92.
5. Okayasu I, Yamada M, Mikami T, Yoshida T, Kanno J, Ohkusa T. Dysplasia and carcinoma development in a repeated dextran sulfate sodium-induced colitis model. J Gastroenterol Hepatol. 2002;17:1078–83.
6. Kuhn R, Lohler J, Rennick D, Rajewsky K, Muller W. Interleukin-10-deficient mice develop chronic enterocolitis. Cell. 1993;75:263–74.
7. Sellon RK, Tonkonogy S, Schultz M, Dieleman LA, Grenther W, Balish E, et al. Resident enteric bacteria are necessary for development of spontaneous colitis and immune system activation in interleukin-10-deficient mice. Infect Immun. 1998;66:5224–31.
8. Shkoda A, Ruiz PA, Daniel H, Kim SC, Rogler G, Sartor RB, et al. Interleukin-10 blocked endoplasmic reticulum stress in intestinal epithelial cells: impact on chronic inflammation. Gastroenterology. 2007;132:190–207.
9. Ohkusa T, Sato N, Ogihara T, Morita K, Ogawa M, Okayasu I. *Fusobacterium varium* localized in the colonic mucosa of patients with ulcerative colitis stimulates species-specific antibody. J Gastroenterol Hepatol. 2002;17:849–53.
10. Ohkusa T, Yoshida T, Sato N, Watanabe S, Tajiri H, Okayasu I. Commensal bacteria can enter colonic epithelial cells and induce proinflammatory cytokine secretion: a possible pathogenic mechanism of ulcerative colitis. J Med Microbiol. 2009;58:535–45.
11. Ohkusa T, Okayasu I, Ogihara T, Morita K, Ogawa M, Sato N. Induction of experimental ulcerative colitis by *Fusobacterium varium* isolated from colonic mucosa of patients with ulcerative colitis. Gut. 2003;52:79–83.
12. Yoshida T, Haga S, Numata Y, Yamashita K, Mikami T, Ogawa T, et al. Disruption of the p53–p53r2 DNA repair system in ulcerative colitis contributes to colon tumorigenesis. Int J Cancer. 2006;118:1395–403.
13. Ohkusa T, Nomura T, Terai T, Miwa H, Kobayashi O, Hojo M, et al. Effectiveness of antibiotic combination therapy in patients with active ulcerative colitis: a randomized, controlled pilot trial with long-term follow-up. Scand J Gastroenterol. 2005;40:1334–42.
14. Nomura T, Ohkusa T, Okayasu I, Yoshida T, Sakamoto M, Hayashi H, et al. Mucosa-associated bacteria in ulcerative colitis before and after antibiotic combination therapy. Aliment Pharmacol Ther. 2005;21:1017–27.
15. Ohkusa T, Kato K, Terao S, Chiba T, Mabe K, Murakami K, et al. Newly developed antibiotic combination therapy for ulcerative colitis: a double-blind placebo-controlled multicenter trial. Am J Gastroenterol. 2010;105:1820–9.
16. Yamashita K, Yasuda S, Kuba T, Otani Y, Fujiwara M, Okayasu I. Unique characteristics of rectal carcinoma cell lines derived from invasive carcinomas in ulcerative colitis patients. Cancer Sci. 2004;95:211–7.
17. Kanno J, Aisaki K, Igarashi K, Nakatsu N, Ono A, Kodama Y, et al. "Per cell" normalization method for mRNA measurement by quantitative PCR and microarrays. BMC Genomics. 2006;7:64.
18. Leung MK, Jones T, Michels CL, Livingston DM, Bhattacharya S. Molecular cloning and chromosomal localization of the human CITED2 gene encoding p35srj/Mrg1. Genomics. 1999;61:307–13.
19. Sanosaka T, Namihira M, Asano H, Kohyama J, Aisaki K, Igarashi K, et al. Identification of genes that restrict astrocyte differentiation of midgestational neural precursor cells. Neuroscience. 2008;155:780–8.
20. Aisaki K, Aizawa S, Fujii H, Kanno J, Kanno H. Glycolytic inhibition by mutation of pyruvate kinase gene increases oxidative stress and causes apoptosis of a pyruvate kinase deficient cell line. Exp Hematol. 2007;35:1190–200.
21. Matts SG. The value of rectal biopsy in the diagnosis of ulcerative colitis. Q J Med. 1961;30:393–407.
22. Sinicrope FA, Lemoine M, Xi L, Lynch PM, Cleary KR, Shen Y, et al. Reduced expression of cyclooxygenase 2 proteins in hereditary nonpolyposis colorectal cancers relative to sporadic cancers. Gastroenterology. 1999;117:350–8.
23. Braganca J, Eloranta JJ, Bamforth SD, Ibbitt JC, Hurst HC, Bhattacharya S. Physical and functional interactions among AP-2 transcription factors, p300/CREB-binding protein, and CITED2. J Biol Chem. 2003;278:16021–9.

24. Kruse JP, Gu W. Modes of p53 regulation. Cell. 2009;137: 609–22.
25. Lowe SW, Ruley HE, Jacks T, Housman DE. p53-dependent apoptosis modulates the cytotoxicity of anticancer agents. Cell. 1993;74:957–67.
26. Vousden KH, Prives C. Blinded by the light: the growing complexity of p53. Cell. 2009;137:413–31.
27. Yoshida T, Mikami T, Mitomi H, Okayasu I. Diverse p53 alterations in ulcerative colitis-associated low-grade dysplasia: full-length gene sequencing in microdissected single crypts. J Pathol. 2003;199:166–75.
28. Scheppach W. Effects of short chain fatty acids on gut morphology and function. Gut. 1994;35:S35–8.
29. Sperling S, Grimm CH, Dunkel I, Mebus S, Sperling HP, Ebner A, et al. Identification and functional analysis of CITED2 mutations in patients with congenital heart defects. Hum Mutat. 2005;26:575–82.
30. Qu X, Lam E, Doughman YQ, Chen Y, Chou YT, Lam M, et al. Cited2, a coactivator of HNF4alpha, is essential for liver development. EMBO J. 2007;26:4445–56.
31. Bhattacharya S, Michels CL, Leung MK, Arany ZP, Kung AL, Livingston DM. Functional role of p35srj, a novel p300/CBP binding protein, during transactivation by HIF-1. Genes Dev. 1999;13:64–75.
32. Bakker WJ, Harris IS, Mak TW. FOXO3a is activated in response to hypoxic stress and inhibits HIF1-induced apoptosis via regulation of CITED2. Mol Cell. 2007;28:941–53.
33. Suzuki H, Tomida A, Tsuruo T. Dephosphorylated hypoxia-inducible factor 1alpha as a mediator of p53-dependent apoptosis during hypoxia. Oncogene. 2001;20:5779–88.
34. Harris AL. Hypoxia—a key regulatory factor in tumour growth. Nat Rev Cancer. 2002;2:38–47.
35. Greijer AE, van der Wall E. The role of hypoxia inducible factor 1 (HIF-1) in hypoxia induced apoptosis. J Clin Pathol. 2004;57: 1009–14.
36. Sowter HM, Ratcliffe PJ, Watson P, Greenberg AH, Harris AL. HIF-1-dependent regulation of hypoxic induction of the cell death factors BNIP3 and NIX in human tumors. Cancer Res. 2001; 61:6669–73.
37. Garcia CK, Li X, Luna J, Francke U. cDNA cloning of the human monocarboxylate transporter 1 and chromosomal localization of the SLC16A1 locus to 1p13.2–p12. Genomics. 1994;23:500–3.
38. Cuff M, Dyer J, Jones M, Shirazi-Beechey S. The human colonic monocarboxylate transporter Isoform 1: its potential importance to colonic tissue homeostasis. Gastroenterology. 2005;128:676–86.
39. Gu W, Roeder RG. Activation of p53 sequence-specific DNA binding by acetylation of the p53 C-terminal domain. Cell. 1997;90:595–606.
40. Yoshida T, Matsumoto N, Mikami T, Okayasu I. Upregulation of p16(INK4A) and Bax in p53 wild/p53-overexpressing crypts in ulcerative colitis-associated tumours. Br J Cancer. 2004;91: 1081–8.
41. Ohkusa T, Okayasu I, Tokoi S, Ozaki Y. Bacterial invasion into the colonic mucosa in ulcerative colitis. J Gastroenterol Hepatol. 1993;8:116–8.

BIOLOGY OF REPRODUCTION 84, 734–742 (2011)
Published online before print 1 December 2010.
DOI 10.1095/biolreprod.110.087502

Endocrine Disrupter Bisphenol A Increases In Situ Estrogen Production in the Mouse Urogenital Sinus[1]

Shigeki Arase,[3,5] Kenichiro Ishii,[3,4,5] Katsuhide Igarashi,[6] Kenichi Aisaki,[6] Yuko Yoshio,[5] Ayami Matsushima,[7] Yasuyuki Shimohigashi,[7] Kiminobu Arima,[5] Jun Kanno,[6] and Yoshiki Sugimura[2,5]

Department of Nephro-Urologic Surgery and Andrology,[5] Mie University Graduate School of Medicine, Mie, Japan
Division of Cellular & Molecular Toxicology,[6] National Institute of Health Sciences, Tokyo, Japan
Laboratory of Structure-Function Biochemistry,[7] Department of Chemistry, Faculty of Sciences, Kyushu University, Fukuoka, Japan

ABSTRACT

The balance between androgens and estrogens is very important in the development of the prostate, and even small changes in estrogen levels, including those of estrogen-mimicking chemicals, can lead to serious changes. Bisphenol A (BPA), an endocrine-disrupting chemical, is a well-known, ubiquitous, estrogenic chemical. To investigate the effects of fetal exposure to low-dose BPA on the development of the prostate, we examined alterations of the in situ sex steroid hormonal environment in the mouse urogenital sinus (UGS). In the BPA-treated UGS, estradiol (E_2) levels and CYP19A1 (cytochrome P450 aromatase) activity were significantly increased compared with those of the untreated and diethylstilbestrol (DES)-treated UGS. The mRNAs of steroidogenic enzymes, *Cyp19a1* and *Cyp11a1*, and the sex-determining gene, *Nr5a1*, were up-regulated specifically in the BPA-treated group. The up-regulation of mRNAs was observed in the mesenchymal component of the UGS as well as in the cerebellum, heart, kidney, and ovary but not in the testis. The number of aromatase-expressing mesenchymal cells in the BPA-treated UGS was approximately twice that in the untreated and DES-treated UGS. The up-regulation of *Esrrg* mRNA was observed in organs for which mRNAs of steroidogenic enzymes were also up-regulated. We demonstrate here that fetal exposure to low-dose BPA has the unique action of increasing in situ E_2 levels and CYP19A1 (aromatase) activity in the mouse UGS. Our data suggest that BPA might interact with in situ steroidogenesis by altering tissue components, such as the accumulation of aromatase-expressing mesenchymal cells, in particular organs.

aromatase, bisphenol A, developmental biology, embryo, estradiol/estrogen receptor, in situ estrogen production, male reproductive tract, prostate, steroidogenic enzyme, urogenital sinus

INTRODUCTION

Endocrine-disrupting chemicals (EDCs) have been implicated in the alteration of fetal development of urogenital organs as well as the reproductive and endocrine systems in humans and other species [1]. The fetal development of urogenital organs is induced by endogenous hormonal messages that originate in fetal and maternal hormone systems. Fetal exposure to EDCs disrupts the interactions between endogenous hormones and their receptors, causing adverse effects later in life [2]. In the prostate, both androgens and estrogens play a significant role in development and differentiation as well as in the maintenance of adult homeostasis [3]. Therefore, even small changes in estrogen levels, including those of estrogen-mimicking chemicals, can lead to changes in prostate development and differentiation.

Bisphenol A (BPA), one of the EDCs, is a well-known, ubiquitous, estrogenic chemical used in the manufacture of polycarbonate plastics, as a lining in metal food and drink cans, and in dental sealants [4]. The concern with BPA originates from its detection in maternal and fetal plasma as well as the placenta [5, 6]. Thus, fetal exposure to BPA is implicated in fetal toxicity as well as in subsequent growth of the infant. Histopathologically, fetal exposure to low-dose BPA (10 μg kg^{-1} day^{-1}) has been shown to increase cell proliferation of urogenital sinus epithelium (UGE) in the primary prostatic ducts of CD1 mice [7]. Recently, our group reported that fetal exposure to low-dose BPA (20 μg kg^{-1} day^{-1}) specifically increased the number of basal epithelial cells in the adult prostate of BALB/c mice and also induced permanent cytokeratin 10 expression in such cells similar to the effects of synthetic estrogen diethylstilbestrol (DES; 0.2 μg kg^{-1} day^{-1}) [8]. Epigenetically, neonatal exposure of male rats to low-dose BPA (10 μg kg^{-1} day^{-1}) elicited critical molecular changes during prostate development and also increased prostatic gland susceptibility to precancerous neoplastic lesions and hormonal carcinogenesis [9]. Toxicological studies of BPA at less than 50 μg kg^{-1} day^{-1} in rodent fetuses and offspring have demonstrated alterations of mammary gland development, open-field behavior, and reproductive functioning [10–12].

Some EDCs are reported to alter the in situ sex steroid hormonal environment in the reproductive system. The triazine herbicide atrazine binds directly to adrenal-4-binding protein/steroidogenic factor-1 (official symbol NR5A1) and increases CYP19A1 (cytochrome P450 aromatase) expression and, ultimately, estradiol (E_2) production in human genital cancer cell lines [13]. The aryl hydrocarbon (dioxin) also increases CYP19A1 (aromatase) expression mediated by its receptor in mouse ovaries [14]. In contrast, the phosphorothioate insecticide profenofos increases the expression of steroidogenic genes

[1]Supported by Grants-in-Aid from the Ministry of Health, Labor, and Welfare, Japan. GEO accession no. GSE24928.
[2]Correspondence: Yoshiki Sugimura, Department of Nephro-Urologic Surgery and Andrology, Mie University Graduate School of Medicine, 2-174 Edobashi, Tsu, Mie 514-8507, Japan. FAX: 81 59 231 5203; e-mail: sugimura@clin.medic.mie-u.ac.jp
[3]These authors contributed equally to this work.
[4]Current address: Mie University Graduate School of Regional Innovation Studies, 1577 kurimamachiya-cho, Tsu, Mie 514-8507, Japan.

Received: 27 July 2010.
First decision: 19 August 2010.
Accepted: 15 November 2010.

eISSN: 1529-7268 http://www.biolreprod.org
ISSN: 0006-3363

and testosterone levels in rat testes [15]. Recently reported adverse effects of BPA on in situ steroidogenesis include increased testosterone levels in mouse Leydig cells and decreased E_2 levels in porcine ovarian granulosa cells [16, 17]. Thus, BPA may have the potential not only to mimic estrogenic action but also to alter in situ steroidogenesis in the prostate as well as other reproductive organs.

To investigate the effects of fetal exposure to low-dose BPA on in situ steroidogenesis in the developing prostate, we first measured sex steroid hormone levels and CYP19A1 (aromatase) activity in the BPA-treated mouse urogenital sinus (UGS), from which the prostate develops embryologically. Subsequently, we examined the alterations of steroidogenic enzyme gene expression to confirm the alterations of the in situ sex steroid hormonal environment in the BPA-treated mouse UGS. Finally, we identified the BPA-specific biological effects for in situ steroidogenesis during fetal prostate development.

MATERIALS AND METHODS

Animals

In the present study, 36 pregnant female C57BL/6 mice were purchased on the 12th day of gestation from Japan SLC, where the breeding strategy was to mate three female C57BL/6 mice (age, 10 wk) with one male overnight and separate them the next morning (plug date denoted as Day 0). All animals were housed individually in chip-bedded polyolefin cages in a room with controlled temperature (23 ± 1°C) and humidity (45 to 65%) on a 12L:12D photoperiod. Mice were fed a low-phytoestrogen diet (NIH-07PLD; Oriental Yeast Co.) and tap water ad libitum.

Chemicals

For the present study, both BPA and DES with a purity of 99% or greater were purchased from Nacalai Tesque and Wako Pure Chemical Industries, respectively.

Fetal Exposure to Chemicals

We randomly assigned 36 pregnant female C57BL/6 mice to three different treatment groups: BPA (20 μg kg^{-1} day^{-1}, n = 12) or DES (0.2 μg kg^{-1} day^{-1}, n = 12), both of which were dissolved in tocopherol-stripped corn oil (MP Biomedical, Inc.), administered by oral gavages on Embryonic Day (E) 13 to E16 and the control group, in which pregnant mice were fed tocopherol-stripped corn oil (2 ml/kg, n = 12). Previously, our group reported that this protocol of fetal exposure to BPA and DES resulted in similar histopathological changes of adult prostate—that is, increased basal epithelial cell number and induction of cytokeratin 10, a classic marker associated with squamous differentiation, in such cells [8]. Our dose level of BPA for the present study was also based on reported results suggesting that BPA is less than 100-fold less potent than DES. The Mie University's Committee on Animal Investigation approved the experimental protocol.

Termination and UGS Dissection

Between E17 and Postnatal Day (P) 1, all animals were terminated by an overdose of isoflurane followed by cervical dislocation. For each of the three groups, from 15 to 18 fetuses (both male and female) from three pregnant mice were collected at E17, E18, P0, and P1. The bladder and urethra were removed and dissected to isolate the UGS, and then the five or six UGS obtained were pooled as one sample. Thus, the 15–18 UGS were divided into three samples at each time point. The UGS, cerebellum, heart, kidney, testis, and ovary were collected in RNAlater (Applied Biosystems).

To isolate pure UGS, other tissues, such as the bladder, urethra, wolffian duct, seminal vesicle, and mullerian duct, were removed from both the male and female urogenital tracts. The histopathology of the mouse UGS was then examined by hematoxylin-and-eosin staining.

Measurements of In Situ E_2 Levels and CYP19A1 (Aromatase) Activity in UGS

The E_2 levels and CYP19A1 (aromatase) activity in UGS were determined by liquid chromatography-tandem mass spectrometry [18] and a tritiated water release assay [19], respectively, which were made available by Aska Pharma Medical. Briefly, the organs were homogenized, and the extracts were applied to a C18 Amprep solid-phase column (Amersham Biosciences) to remove contaminating fats. The E_2 was then separated using a normal-phase high-performance liquid chromatography system (Jasco) with a silica gel column (Cosmosil 5SI; Nacalai Tesque), and 100 pg of isotope-labeled [$^{13}C_4$]E_2 were added to extracts. The evaporated extracts were reacted with 5% pentafluorobenzyl bromide/acetonitrile, under KOH/ethanol, for 1 h at 55°C. After evaporation, the products were reacted with 100 ml of picolinic acid solution (2% picolinic acid, 2% 2-dimethylaminopyridinc, and 1% 2-methyl-6-nitrobenzoic acid in tetrahydrofuran) and 20 ml of triethylamine for 0.5 h at room temperature. The reaction products were dissolved in 1% acetic acid and then purified using a Bond Elute C18 column (Varian). The products were measured with a reverse-phase liquid chromatograph (Agilent 1100; Agilent Technologies) coupled with an API 5000 triple-stage quadrupole mass spectrometer (Applied Biosystems) in the positive-ion mode. This device monitored the *m/z* 558 to *m/z* 339 (E_2) and *m/z* 562 to *m/z* 343 ([$^{13}C_4$]E_2) transitions.

The tritiated water release assay was used for the measurement of CYP19A1 (aromatase) activity. This method measures the production of ^3H_2O, which forms as a result of aromatization of the substrate [1b-^{3}H]androst-4-ene-3,17-dione (New England Nuclear). Serum-free medium containing [1b-^{3}H]androst-4-ene-3,17-dione solution (54 nM) was prepared, of which 0.5 ml was added to each sample. After incubation for 1 h, the samples were placed on ice, and 200 μl of culture medium were withdrawn. The medium was extracted with 500 μl of chloroform, vortexed, and then centrifuged for 1 min at 9000 × *g*. A 100-μl aliquot of the aqueous phase was mixed with 100 μl of a 5% (wt/vol) charcoal/0.5% (wt/vol) dextran T-70 suspension, vortexed, and then incubated at room temperature for 10 min. Then, after centrifugation of the solution for 5 min at 9000 × *g*, a 150-μl aliquot was removed for measurement of radioactivity by liquid scintillation.

RNA Extraction and cDNA Preparation

Total RNA was extracted using the RNeasy Mini Kit (Qiagen, Inc.) in accordance with the manufacturer's instructions. The RNA concentration was then determined spectrophotometrically by a multidetection microplate reader (Dainippon Sumitomo Pharma Co.). From 50 ng of total RNA, cDNA was reverse transcribed using oligo(dT) and Superscript II RNase H-reverse transcriptase (Invitrogen) as previously described [8].

Analysis of Gene Expression Profile

For determining gene expression profiles of the male UGS, GeneChip analysis with the Percellome method was performed [20]. Briefly, organs were prepared using RLT buffer (Qiagen, Inc.). Total RNA was extracted using RNeasy Mini Kit. First-strand cDNA was synthesized by incubating 5 mg of total RNA with a T7 oligo(dT) primer (Invitrogen) according to the manufacturer's protocol. The dsDNA was mixed with T7 RNA polymerase (Enzo Biochem, Inc.). During the in vitro transcription, generated cRNAs were labeled with biotin-16-UTP and biotin-11-CTP (Enzo Biochem, Inc.). The purified cRNA was fragmented at 300–500 bp into the target solution. Hybridization was performed with the GeneChip Mouse Genome 430 Version 2.0 (Affymetrix, Inc.) at 45°C for 18 h after staining with streptavidin-R-phycoerythrin conjugates (Molecular Probes, Invitrogen). The reacted arrays were then scanned as digital image files, and the scanned data were analyzed with GeneChip Operating Software (Affymetrix, Inc.). The expression data were converted to copy numbers of mRNA per cell by the Percellome method, quality controlled, and analyzed using Percellome software [20].

Real-Time PCR Analysis

Real-time PCR was carried out in the iCycler iQ Detection System (Bio-Rad Laboratories) with iQ SYBR-Green Supermix reagents (Bio-Rad Laboratories) as previously described [8]. The PCR amplification reaction was performed with specific primers as shown in Table 1. After PCR, melting-curve analysis was performed to verify specificity and identity of the PCR products. All data were analyzed with the iCycler iQ Optical System Software Version 3.0A (Bio-Rad Laboratories). All PCR data were normalized to *Gapdh* mRNA.

Preparation of Primary Cultured Mesenchymal Cells from UGS

The UGS were dissected from the fetuses and separated into UGE and urogenital sinus mesenchyme (UGM) by tryptic digestion and mechanical separation as previously described [21]. UGM were cultured in RPMI-1640

TABLE 1. Sequences of oligonucleotide primers used for the real-time PCR analyses.

Gene	Primer[a]
Gapdh	F: 5′-AAATGGTGAAGGTCGGTGTG-3′
	R: 5′-TGAAGGGGTCGTTGATGG-3′
Cyp19a1	F: 5′-GCCCAATGAATTTACCCTCGAA-3′
	R: 5′-AAGCCAAAAGGCTGAAAGTACCT-3′
Cyp11a1	F: 5′-TCGACTCCTCAGAACTAAGACCTG-3′
	R: 5′-GTACCCTGGTGTCCTTTATAGCCT-3′
Nr5a1	F: 5′-CCTGGGCTGGCTACCTCTATC-3′
	R: 5′-CGAACTAGAGCCAGAGGAGGAC-3′
Esr1	F: 5′-GCACAGGATGCTAGCCTTGTCTC-3′
	R: 5′-AATTGTCACCAGCTTGCAGGTTC-3′
Ar	F: 5′-GGCGGTCCTTCACTAATGTCAACT-3′
	R: 5′-CTGACTTGTGCATGCGGTACTCAT-3′
Esrrg	F: 5′-CCGAGAGTTGGTGGTTATCATTGG-3′
	R: 5′-GGAAGACCCTCGCCGTGC-3′

[a] F, forward; R, reverse.

with 5% fetal bovine serum and plated out on four-well glass slides (BD Falcon). After several days, cells were fixed in methanol and processed for immunocytochemical analysis.

Immunocytochemical Staining

The sections were first incubated for 15 min in 0.01 M PBS. After inhibition of endogenous peroxidases (10 min in 0.6% H_2O_2 diluted in 0.01 M PBS plus 0.2% Triton X-100 [PBST]) and saturation (2 h in a 5% normal goat serum solution), sections were incubated overnight at 4°C in a polyclonal affinity-purified antiaromatase antibody or estrogen-related receptor gamma (ESRRG) antibody raised in rabbit against quail recombinant aromatase or ESRRG diluted 1:500 in 0.01 M PBST. The next day, the sections were immersed for 2 h at room temperature in a biotin-conjugated goat anti-rabbit immunoglobulin G (DakoCytomation, Inc.) diluted 1:400 in PBST and then for 2 h in a streptavidin-fluorescein complex (Rhodamine; DakoCytomation, Inc.) diluted 1:50 in PBST. Between each step, sections were extensively rinsed in PBST. The sections were mounted onto microscope slides, coverslipped with a gelatin-based mounting medium, and stored in the dark at 4°C. For double-labeling immunofluorescence, Alexa Fluor 488- or 594-conjugated secondary antibodies were used. Rabbit polyclonal anti-aromatase antibody was kindly provided by Prof. Nobuhiro Harada (Department of Biochemistry, Fujita Health University School of Medicine, Aichi, Japan) [22]. The rabbit polyclonal anti-ESRRG antibody used in the present study was established and characterized as previously reported [23]. The mouse monoclonal anti-Ran antibody (Santa Cruz Biotechnology, Inc.) was used to detect nucleus in cells. Ran, also called TC4, is the small RAS-related protein that is localized in the nucleus.

Statistical Analysis

Results are expressed as the mean ± SD. Differences among the three groups were determined using Student *t*-test with Dunnett multiple comparison. A value of $P < 0.05$ was considered to be statistically significant.

RESULTS

BPA-Specific Increases of E_2 Levels and CYP19A1 (Aromatase) Activity in Mouse UGS

The pregnant mice were exposed to low-dose BPA during the onset of prostatic budding (E13–E16), and the UGS of fetuses were collected during bud elongation (E17–P1). In analyses of in situ sex steroid hormonal environment, E_2 levels and CYP19A1 (aromatase) activity were significantly increased only at P1 in BPA-treated UGS, not at P1 in the DES-treated UGS (Fig. 1). At E17 and P1, both the E_2 levels and CYP19A1 (aromatase) activity in untreated male UGS were not significantly different compared with those in untreated female UGS.

BPA-Specific Up-Regulation of Steroidogenic Enzyme and Sex-Determining Gene mRNA in Mouse UGS

To investigate the BPA-specific gene alterations related to increases of the E_2 levels and aromatase activity, we performed preliminary GeneChip analysis with the Percellome method in the BPA- or DES-treated male UGS at E17 and P1. The results showed BPA-specific mRNA up-regulation of steroidogenic enzymes, such as *Cyp11a1*, *Cyp11b1*, and *Cyp17a1*, and sex-determining factors, such as *Nr5a1*, *Nr0b1*, *Gata4*, and *Amhr2* (data not shown). Furthermore, quantitative PCR analysis confirmed the mRNA up-regulation of *Cyp19a1*, *Cyp11a1*, and *Nr5a1* only in the BPA-treated neonatal (P0 and P1) UGS, not in the DES-treated neonatal UGS (Fig. 2). No difference in mRNA expression levels was found between E17 and P1 when comparing the untreated male UGS to that of the female. In

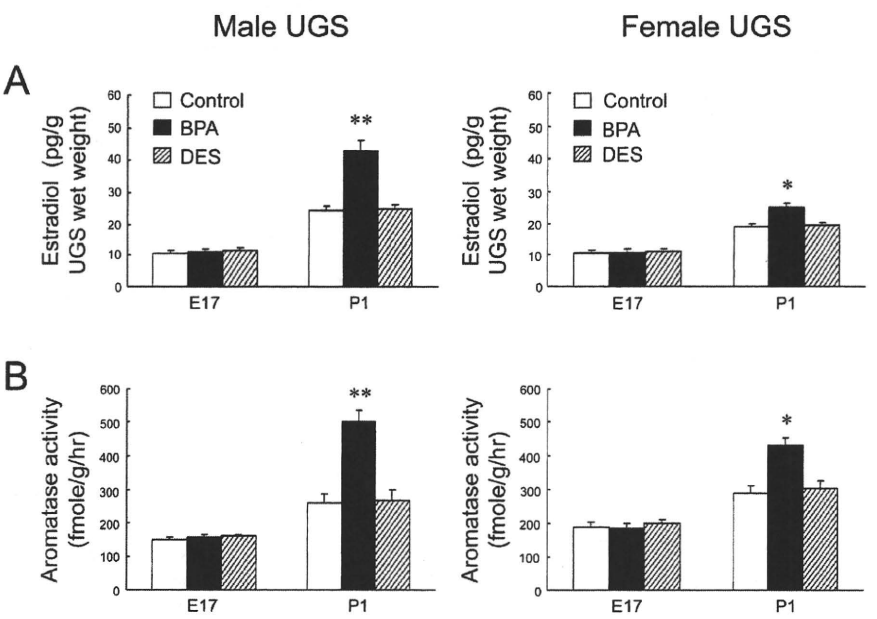

FIG. 1. BPA-specific increases of E_2 levels and CYP19A1 (aromatase) activity in mouse UGS. E_2 levels (**A**) and CYP19A1 (aromatase) activity (**B**) were measured in the untreated control (open bar), BPA-treated UGS (closed bar), and DES-treated UGS (slashed bar) at E17 and P1. $*P < 0.01$, $**P < 0.001$ vs. control.

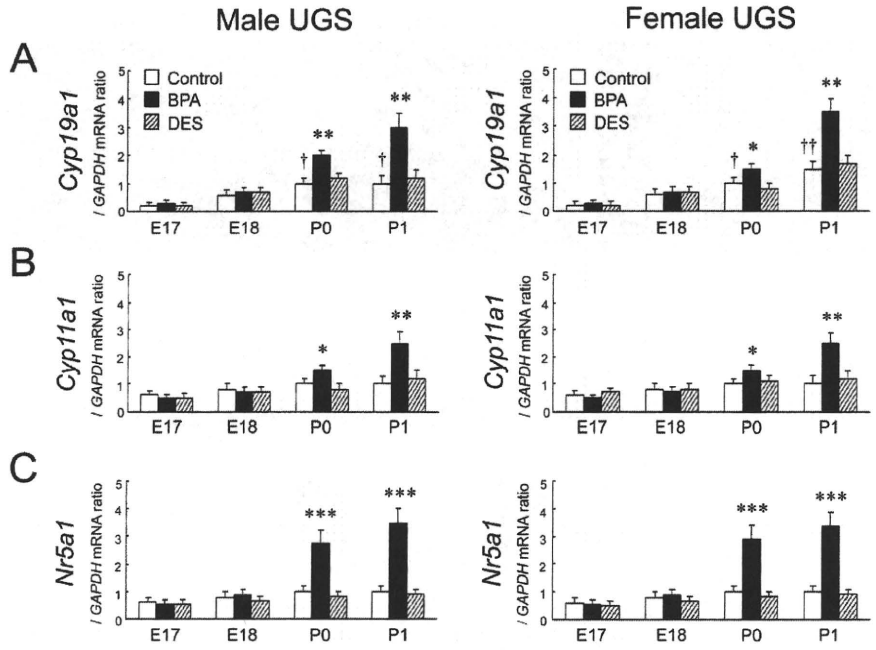

FIG. 2. BPA-specific up-regulation of steroidogenic enzyme and sex-determining gene mRNA in mouse UGS. The relative mRNA expressions of *Cyp19a1* (**A**), *Cyp11a1* (**B**), and *Nr5a1* (**C**) were determined in the untreated control (open bar), BPA-treated UGA (closed bar), and DES-treated UGS (slashed bar) between E17 and P1. $^{*}P < 0.05$, $^{**}P < 0.01$, $^{***}P < 0.001$ vs. control at each time point; $^{\dagger}P < 0.01$, $^{\dagger\dagger}P < 0.001$ vs. control at E17.

untreated male and female UGS, the mRNA of *Cyp19a1* was gradually increased between E17 and P1.

Restricted BPA-Specific Up-Regulation of Steroidogenic Enzyme and Sex-Determining Gene mRNA in UGE and UGM

In male fetuses at P1, it was not feasible to separate UGE and UGM components within the male UGS because of the formation of prostatic buds. In the female at P1, the up-regulation of *Cyp19a1*, *Cyp11a1*, and *Nr5a1* mRNA was observed only in UGM, not in UGE, of the BPA-treated group (Fig. 3). In both male and female UGE, expressions of such mRNAs were quite low and not up-regulated, even in the BPA-treated group. At E17, no difference in mRNA expression levels was found when comparing the untreated male UGM with that of the female.

BPA-Specific Increases of Aromatase-Expressing Cells in Primary Cultured UGM

In both the male and female, P1 UGM was primary cultured in vitro. Representative pictures of aromatase-positive cells are shown in Figure 4, A–C. The aromatase-positive staining was

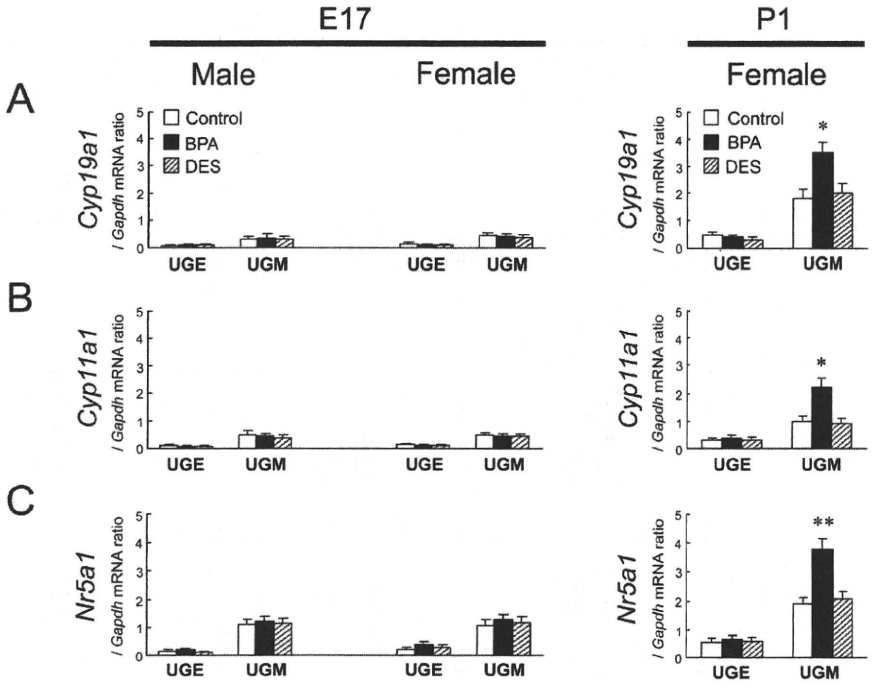

FIG. 3. Restricted BPA-specific up-regulation of steroidogenic enzyme and sex-determining gene mRNA in UGE and UGM. The relative mRNA expressions of *Cyp19a1* (**A**), *Cyp11a1* (**B**), and *Nr5a1* (**C**) were determined for UGE and UGM of the untreated control (open bar), BPA-treated UGS (closed bar), and DES-treated UGS (slashed bar) at E17 and P1. $^{*}P < 0.01$, $^{**}P < 0.001$ vs. control.

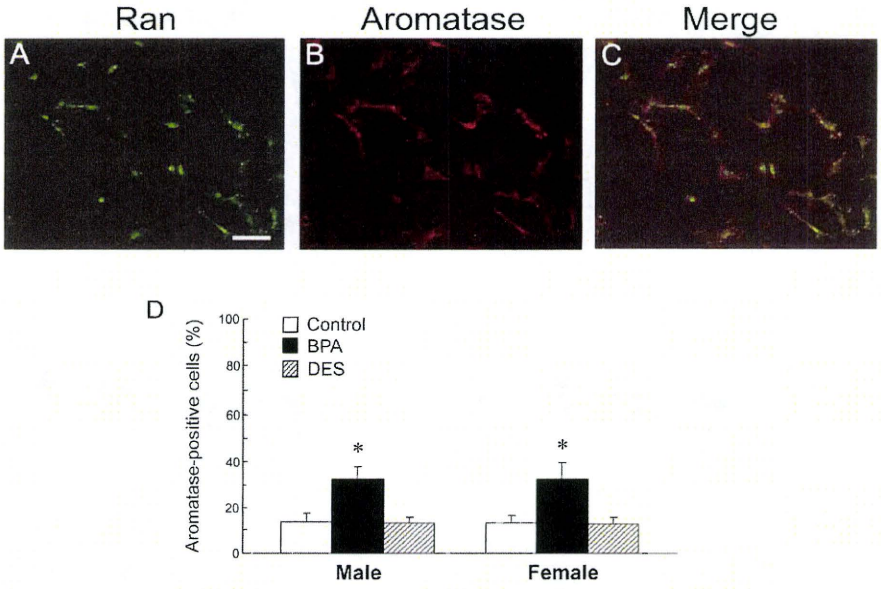

FIG. 4. BPA-specific increases of aromatase-expressing cells in primary cultured UGM. **A–C**) Fluorescence signals were detected for the CYP19A1 (aromatase) protein in primary cultured UGM. The nuclei were identified by Ran staining. Bar = 100 μm, magnification ×400. **D**) The number of aromatase-positive cells was counted in primary cultured UGM of the untreated control open bar), BPA-treated UGS (closed bar), and DES-treated UGS (slashed bar), and the percentage of aromatase-positive cells was calculated from at least 10 areas. $*P < 0.01$ vs. control.

observed in the cytoplasm of cultured UGM. The rate of positivity (i.e., the percentage of cells that expressed CYP19A1 [aromatase] protein), was approximately 10% in the untreated and the DES-treated groups, whereas it was as high as approximately 30% in the BPA-treated group (Fig. 4D). No difference in the rate of positivity of CYP19A1 (aromatase) was found when comparing the untreated male UGM to that of the female.

Restricted BPA-Specific Up-Regulation of Esrrg *mRNA in UGE and UGM*

In E17 female UGM, the mRNA expression of *Esr1* was up-regulated by both BPA and DES treatment (Fig. 5A). At E17, however, the mRNA expression of *Ar* was up-regulated by both BPA and DES treatment in the male UGS (Fig. 5B). At P1, mRNA expression of *Ar* was up-regulated by both BPA and DES treatment in the female UGS (Fig. 5B). In both the male and female, the up-regulation of *Esrrg* mRNA was observed at E17 and restricted in UGM, but not in UGE, of the BPA-treated group (Fig. 5C). In both the male and female UGE, the expression of *Esrrg* mRNA was quite low and not up-regulated, even in the BPA-treated group. At E17, no difference in mRNA expression levels was found when comparing the untreated male UGS with that of the female.

BPA-Specific Increases of ESRRG-Expressing Cells in Primary Cultured UGM

In both the male and female, E17 UGM was primary cultured in vitro. Representative pictures of ESRRG-positive

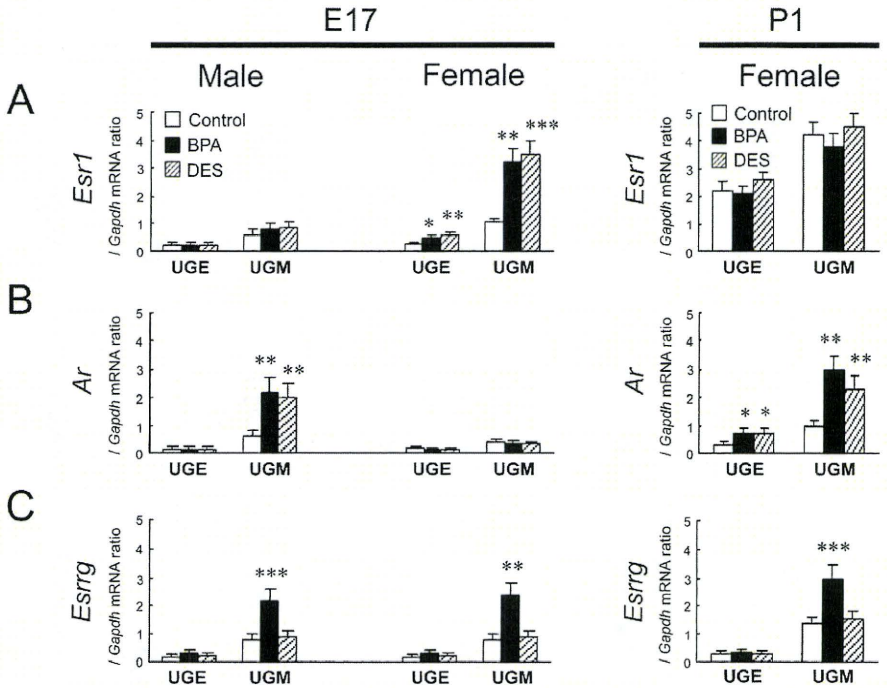

FIG. 5. Restricted BPA-specific up-regulation of *Esrrg* mRNA in UGE and UGM. The relative mRNA expressions of *Esr1* (**A**), *Ar* (**B**), and *Esrrg* (**C**) were determined in UGE and UGM of the untreated control (open bar), BPA-treated UGS (closed bar), and DES-treated UGS (slashed bar) at E17 and P1. $*P < 0.05$, $**P < 0.01$, $***P < 0.001$ vs. control.

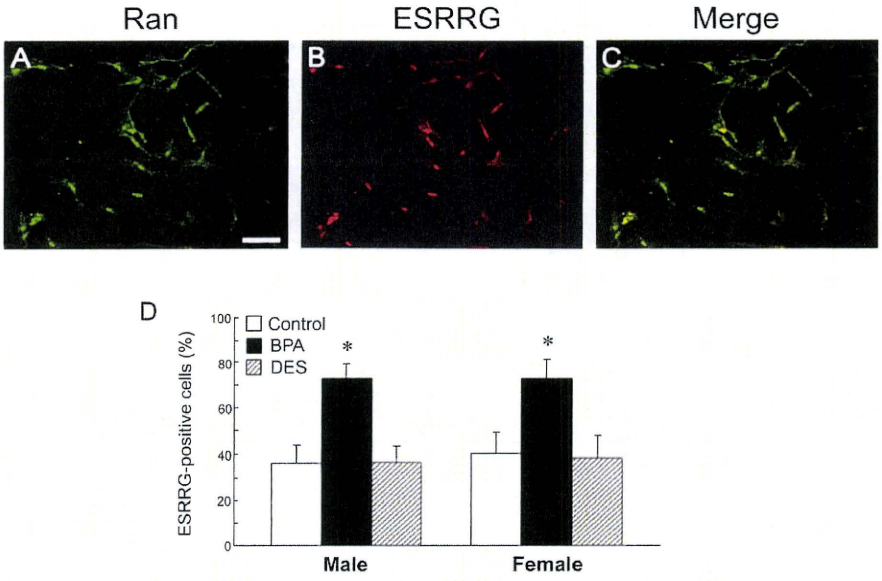

FIG. 6. BPA-specific increases of ESRRG-expressing cells in primary cultured UGM. **A–C**) Fluorescence signals were detected for the ESRRG protein in primary cultured UGM. The nuclei were identified by Ran staining. Bar = 100 μm, magnification ×400. **D**) The number of ESRRG-positive cells was counted in primary cultured UGM of the untreated control (open bar), BPA-treated UGS (closed bar), and DES-treated UGS (slashed bar), and the percentage of ESRRG-positive cells was calculated from at least 10 areas. $*P < 0.01$ vs. control.

cells are shown in Figure 6, A–C. The ESRRG-positive staining was observed in both the nucleus and the cytoplasm of cultured UGM. The number of ESRRG-positive UGM was significantly increased only in the BPA-treated group and showed a 2.2-fold increase in males and a 1.6-fold increase in females (Fig. 6D). No difference was found in the rate of positivity of ESRRG when comparing the untreated male UGM with that of the female.

BPA-Specific Up-Regulation of Esrrg *and Steroidogenic Enzyme mRNA in Sex Hormone-Related Organs*

To investigate the BPA-specific up-regulation of in situ steroidogenesis in other organs, we first examined the changes in *Esrrg* mRNA expression in sex hormone-related organs, such as the cerebellum, heart, kidney, ovary, and testis. At P1, the mRNA expression of *Esr1* in the cerebellum, heart, kidney, and ovary, but not in the testis, was up-regulated by both BPA and DES treatment (Fig. 7A). However, no significant difference in *Ar* mRNA expression was observed in all organs examined (Fig. 7B). In the untreated group, the mRNA expression of *Esrrg* was not detected in the testis at E17 and P1 (Fig. 7C). The up-regulation of *Esrrg* mRNA was observed at E17 and restricted to the cerebellum, heart, kidney, and ovary (Fig. 7C). The BPA-specific up-regulation of *Cyp19a1*, *Cyp11a1*, and *Nr5a1* mRNA was observed only at P1 in the cerebellum, heart, kidney, and ovary, but not in the testis (Fig. 8).

DISCUSSION

Concern about the effects of EDCs such as BPA on human health has been increasing [24]. Although the majority of EDCs have the potential to alter functioning of the reproductive and endocrine system, the actual mechanism responsible for such alterations has not been identified thoroughly. BPA is of concern because its chemical structure resembles that of DES. Several studies have reported that BPA can mimic estrogen action, such as induction of vaginal cornification, uterine vascular permeability, growth and differentiation of the mammary gland, and synaptic plasticity in the hippocampus [25–28]. In the prostate, alterations in normal development can produce permanent changes that persist throughout adulthood and may increase the risk of disease in later life [9]. Thus, our objective was to investigate the biological effects of low-dose BPA on the initial development of primary ducts in the fetal prostate.

During prostatic development, alteration of sex steroid hormone synthesis may be responsible for prostatic anomalies associated with fetal exposure to EDCs. In the present study, fetal exposure to low-dose BPA increased E_2 levels in P1 UGS of both the male and female, whereas DES-induced changes were not detected. This alteration was also correlated with increased activity of CYP19A1 (aromatase) in UGS at P1, suggesting the unique action of BPA for in situ steroidogenesis in UGS. The BPA-specific increase of E_2 levels in UGS at P1 was correlated with the following: mRNA up-regulation of steroidogenic enzymes, such as *Cyp19a1* and *Cyp11a1*, and an increased number of aromatase-expressing UGM. The enzyme CYP19A1 (aromatase) is responsible for in situ E_2 production and the crucial testosterone/E_2 balance necessary for normal embryonic and fetal development, even in males. The data presented here shows that the up-regulation of *Cyp19a1* mRNA in BPA-treated UGM was comparable to changes in both in situ E_2 production and CYP19A1 (aromatase) activity.

In the present study, we demonstrated that the BPA-specific increase in steroidogenic enzyme mRNA and aromatase-expressing cell number were observed in both the male and female UGM. During embryonic development, the mesenchymal component is involved in the induction and organogenesis of various organs, including the prostate, mammary gland, lung, kidney, and pancreas. It has been well established that subpopulations of the mesenchymal component are a source of potent molecules that regulate epithelial growth and differentiation [29]. In the prostate, androgen-responsive signals derived from UGM permissively and instructively induce UGE to form primary ducts of the prostate [30].

Comparison between the neonatal male and female UGS shows a similarity in the condensed mesenchyme of the ventral areas—that is, the ventral prostate mesenchyme (VPM) in the male and the ventral mesenchymal pad (VMP) in the female [31]. In the male, a defined VPM is specifically associated with ductal branching morphogenesis and cytodifferentiation of the ventral prostate. Females do not usually form a prostate. In a

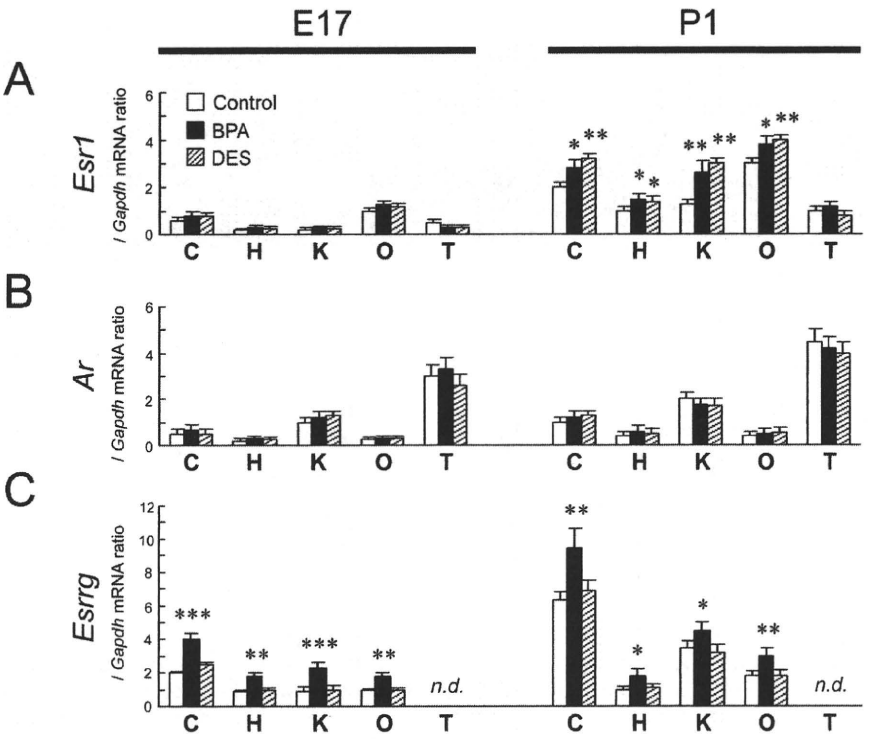

FIG. 7. BPA-specific up-regulation of *Esrrg* mRNA in sex steroid hormone-related organs. The relative mRNA expressions of *Esr1* (**A**), *Ar* (**B**), and *Esrrg* (**C**) were determined in sex steroid hormone-related organs of the untreated control (open bar), BPA-treated UGS (closed bar), and DES-treated UGS (slashed bar) at E17 and P1. C, cerebellum; H, heart; K, kidney; O, ovary; T, testis; *n.d.*, not detected. $*P < 0.05$, $**P < 0.01$, $***P < 0.001$ vs. control.

tissue recombination model, the female VMP induces prostate development in response to androgens [32], suggesting that cells within the female VMP have prostatic-inductive activity. Moreover, an earlier tissue recombination study showed that the ability of the female UGS to respond to androgens in forming prostate was gradually lost between P1 and P5 [33]. These results suggest strongly that androgen-responsive regulatory molecules are expressed constitutively even in the female VMP. Although the female VMP forms in the absence of androgens, androgen receptor (AR) expression was observed in the neonatal female VMP in a pattern similar to that observed in the male VPM [34]. Therefore, the BPA-specific increase in E_2 levels might interact with the intracellular AR signaling in both the male VPM and the female VMP. However, to our knowledge,

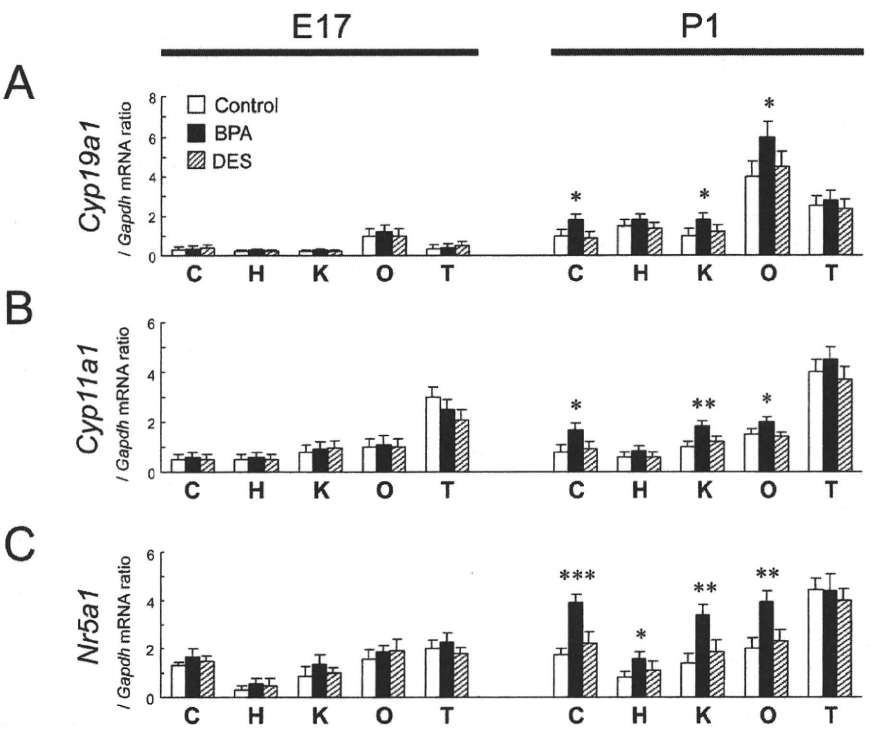

FIG. 8. BPA-specific up-regulation of steroidogenic enzyme and sex-determining gene mRNA in sex steroid hormone-related organs. The relative mRNA expressions of *Cyp19a1* (**A**), *Cyp11a1* (**B**), and *Nr5a1* (**C**) were determined in sex steroid hormone-related organs of the untreated control (open bar), BPA-treated UGS (closed bar), and DES-treated UGS (slashed bar) at E17 and P1. C, cerebellum; H, heart; K, kidney; O, ovary; T, testis. $*P < 0.05$, $**P < 0.01$, $***P < 0.001$ vs. control.

the morphological changes in neonatal female UGS have not yet been investigated.

Our results suggest that BPA has a stimulatory effect on in situ steroidogenesis in P1 UGS of both the male and female at low-dose exposure levels. Recently, ESRRG has been reported to bind strongly with BPA [35]. Susens et al. [36] have reported that expression of ESRRG in the mouse is organ-specific: ESRRG is expressed in the brain, heart, kidney, and skeletal muscle but not in the lung, spleen, and testis. In the present study, the up-regulation of *Cyp19a1* and *Cyp11a1* mRNA by BPA treatment was detected only in organs expressing *Esrrg* mRNA. These data suggest that the possibility of a stimulatory effect on in situ steroidogenesis by fetal exposure to low-dose BPA may be a concern not only in UGS but also in organs expressing ESRRG, such as the brain, heart, kidney, and ovary. It is important to note that Takeda et al. [23] have recently reported that ESRRG was detected in the human testis, suggesting that the distribution of ESRRG differs slightly between mice and humans.

In the present study, the BPA-specific up-regulation of steroidogenic enzyme mRNA in UGS, cerebellum, heart, kidney, and ovary was observed only during the neonatal period (i.e., P0 and P1) and not during the prenatal period (i.e., E17 and E18). During pregnancy in rodents, large amounts of estrogens produced in the maternal ovaries are continuously delivered to the fetus through the placenta. After birth, however, the fetus may be released from the maternal, high-estrogen environment. Thus, one possibility is that the maternal, high-estrogen environment in pregnancy may protect the fetus from the effect of BPA on in situ steroidogenesis during the prenatal period. However, we did not investigate the effects of neonatal BPA treatment on in situ steroidogenesis.

The EDC-induced alterations of the in situ estrogen environment depend on each compound. In addition to atrazine and dioxin, the organotin compound tributyltin also increases E_2 production in human placental choriocarcinoma cells [37]. Tributyltin has been demonstrated to induce the superimposition of male sex organs, such as a penis and/or a vas deferens, over female sex organs, which is a phenomenon known as imposex [38]. These studies suggest strongly that EDCs might affect fetal development not only by mimicking the actions of sex steroid hormones but also by alteration of in situ steroidogenesis.

In the prostate, AR expressed in mesenchyme is required for directing growth and branching morphogenesis of epithelia, presumably by induction of growth factors [39]. In the present study, fetal exposure to BPA or DES increased *Ar* mRNA expression in E17 UGM of the male, whereas *Esr1* mRNA expression was up-regulated in E17 UGM of the female. Recently, Richter et al. [40] have reported that in vitro BPA treatment stimulates *Ar* and *Esr1* mRNA expression in mesenchymal cells isolated from fetal mouse prostate. Thus, our results support the idea that BPA-induced cell proliferation of the primary prostatic ducts may be caused by inducing *Ar* mRNA expression in the male UGM. In contrast, the induction of *Esr1* mRNA expression by BPA or DES may create a positive-feedback loop in the female UGM. Further investigation and morphological analysis will be necessary to confirm the effects of up-regulated ESR1 in the female UGS.

In conclusion, we have shown the unique action of BPA in the mouse UGS. Specifically, we have demonstrated that the increases in E_2 levels and CYP19A1 (aromatase) activity were observed in the BPA-treated UGS but not in the DES-treated UGS. Ricke et al. [41] have recently reported that stromal hormone imbalance, a potential source of local E_2 production, may be responsible for prostatic disease, such as benign prostatic hyperplasia and prostate cancer. The data in the present study give rise to the concept that the development and differentiation of UGS in mouse fetuses is very sensitive to fetal exposure to low-dose BPA via the mother. Further investigation of various aspects of BPA-specific action is necessary to fully understand the role of BPA as an EDC.

ACKNOWLEDGMENTS

We thank Prof. Nobuhiro Harada at Department of Biochemistry, Fujita Health University School of Medicine, Aichi, Japan, for kindly providing rabbit polyclonal antiaromatase antibody. We also thank Mrs. Hiroko Nishii for technical support.

REFERENCES

1. Sekizawa J. Low-dose effects of bisphenol A: a serious threat to human health? J Toxicol Sci 2008; 33:389–403.
2. Newbold RR, Jefferson WN, Padilla-Banks E. Prenatal exposure to bisphenol A at environmentally relevant doses adversely affects the murine female reproductive tract later in life. Environ Health Perspect 2009; 117:879–885.
3. McPherson SJ, Ellem SJ, Risbridger GP. Estrogen-regulated development and differentiation of the prostate. Differentiation 2008; 76:660–670.
4. Welshons WV, Nagel SC, vom Saal FS. Large effects from small exposures. III. Endocrine mechanisms mediating effects of bisphenol A at levels of human exposure. Endocrinology 2006; 147:S56–S69.
5. Schonfelder G, Wittfoht W, Hopp H, Talsness CE, Paul M, Chahoud I. Parent bisphenol A accumulation in the human maternal-fetal-placental unit. Environ Health Perspect 2002; 110:A703–A707.
6. Tsutsumi O. Assessment of human contamination of estrogenic endocrine-disrupting chemicals and their risk for human reproduction. J Steroid Biochem Mol Biol 2005; 93:325–330.
7. Timms BG, Howdeshell KL, Barton L, Bradley S, Richter CA, vom Saal FS. Estrogenic chemicals in plastic and oral contraceptives disrupt development of the fetal mouse prostate and urethra. Proc Natl Acad Sci U S A 2005; 102:7014–7019.
8. Ogura Y, Ishii K, Kanda H, Kanai M, Arima K, Wang Y, Sugimura Y. Bisphenol A induces permanent squamous change in mouse prostatic epithelium. Differentiation 2007; 75:745–756.
9. Ho SM, Tang WY, Belmonte de Frausto J, Prins GS. Developmental exposure to estradiol and bisphenol A increases susceptibility to prostate carcinogenesis and epigenetically regulates phosphodiesterase type 4 variant 4. Cancer Res 2006; 66:5624–5632.
10. Markey CM, Luque EH, Munoz de Toro M, Sonnenschein C, Soto AM. In utero exposure to bisphenol A alters the development and tissue organization of the mouse mammary gland. Biol Reprod 2001; 65: 1215–1223.
11. Honma S, Suzuki A, Buchanan DL, Katsu Y, Watanabe H, Iguchi T. Low-dose effect of in utero exposure to bisphenol A and diethylstilbestrol on female mouse reproduction. Reprod Toxicol 2002; 16:117–122.
12. Kubo K, Arai O, Omura M, Watanabe R, Ogata R, Aou S. Low-dose effects of bisphenol A on sexual differentiation of the brain and behavior in rats. Neurosci Res 2003; 45:345–356.
13. Fan W, Yanase T, Morinaga H, Gondo S, Okabe T, Nomura M, Komatsu T, Morohashi K, Hayes TB, Takayanagi R, Nawata H. Atrazine-induced aromatase expression is SF-1 dependent: implications for endocrine disruption in wildlife and reproductive cancers in humans. Environ Health Perspect 2007; 115:720–727.
14. Baba T, Mimura J, Nakamura N, Harada N, Yamamoto M, Morohashi K, Fujii-Kuriyama Y. Intrinsic function of the aryl hydrocarbon (dioxin) receptor as a key factor in female reproduction. Mol Cell Biol 2005; 25: 10040–10051.
15. Moustafa GG, Ibrahim ZS, Hashimoto Y, Alkelch AM, Sakamoto KQ, Ishizuka M, Fujita S. Testicular toxicity of profenofos in matured male rats. Arch Toxicol 2007; 81:875–881.
16. Song KH, Lee K, Choi HS. Endocrine disrupter bisphenol A induces orphan nuclear receptor Nur77 gene expression and steroidogenesis in mouse testicular Leydig cells. Endocrinology 2002; 143:2208–2215.
17. Mlynarcikova A, Kolena J, Fickova M, Scsukova S. Alterations in steroid hormone production by porcine ovarian granulosa cells caused by bisphenol A and bisphenol A dimethacrylate. Mol Cell Endocrinol 2005; 244:57–62.
18. Hojo Y, Higo S, Ishii H, Ooishi Y, Mukai H, Murakami G, Kominami T, Kimoto T, Honma S, Poirier D, Kawato S. Comparison between

hippocampus-synthesized and circulation-derived sex steroids in the hippocampus. Endocrinology 2009; 150:5106–5112.
19. Nakanishi T, Nishikawa J, Hiromori Y, Yokoyama H, Koyanagi M, Takasuga S, Ishizaki J, Watanabe M, Isa S, Utoguchi N, Itoh N, Kohno Y, et al. Trialkyltin compounds bind retinoid X receptor to alter human placental endocrine functions. Mol Endocrinol 2005; 19:2502–2516.
20. Kanno J, Aisaki K, Igarashi K, Nakatsu N, Ono A, Kodama Y, Nagao T. "Per cell" normalization method for mRNA measurement by quantitative PCR and microarrays. BMC Genomics 2006; 7:64–77.
21. Ishii K, Imanaka-Yoshida K, Yoshida T, Sugimura Y. Role of stromal tenascin-C in mouse prostatic development and epithelial cell differentiation. Dev Biol 2008; 324:310–319.
22. Jakab RL, Horvath TL, Leranth C, Harada N, Naftolin F. Aromatase immunoreactivity in the rat brain: gonadectomy-sensitive hypothalamic neurons and an unresponsive "limbic ring" of the lateral septum-bed nucleus-amygdala complex. J Steroid Biochem Mol Biol 1993; 44:481–498.
23. Takeda Y, Liu X, Sumiyoshi M, Matsushima A, Shimohigashi M, Shimohigashi Y. Placenta expressing the greatest quantity of bisphenol A receptor ERRgamma among the human reproductive tissues: predominant expression of type-1 ERRgamma isoform. J Biochem 2009; 146:113–122.
24. vom Saal FS, Akingbemi BT, Belcher SM, Birnbaum LS, Crain DA, Eriksen M, Farabollini F, Guillette LJ Jr, Hauser R, Heindel JJ, Ho SM, Hunt PA, et al. Chapel Hill Bisphenol A Expert Panel Consensus Statement: integration of mechanisms, effects in animals and potential to impact human health at current levels of exposure. Reprod Toxicol 2007; 24:131–138.
25. Steinmetz R, Mitchner NA, Grant A, Allen DL, Bigsby RM, Ben-Jonathan N. The xenoestrogen bisphenol A induces growth, differentiation, and c-fos gene expression in the female reproductive tract. Endocrinology 1998; 139:2741–2747.
26. Milligan SR, Balasubramanian AV, Kalita JC. Relative potency of xenobiotic estrogens in an acute in vivo mammalian assay. Environ Health Perspect 1998; 106:23–26.
27. Colerangle JB, Roy D. Profound effects of the weak environmental estrogen-like chemical bisphenol A on the growth of the mammary gland of Noble rats. J Steroid Biochem Mol Biol 1997; 60:153–160.
28. Kawato S. Endocrine disrupters as disrupters of brain function: a neurosteroid viewpoint. Environ Sci 2004; 11:1–14.
29. Donjacour AA, Cunha GR. Stromal regulation of epithelial function. Cancer Treat Res 1991; 53:335–364.
30. Hayashi N, Cunha GR, Parker M. Permissive and instructive induction of adult rodent prostatic epithelium by heterotypic urogenital sinus mesenchyme. Epithelial Cell Biol 1993; 2:66–78.
31. Thomson AA. Role of androgens and fibroblast growth factors in prostatic development. Reproduction 2001; 121:187–195.
32. Timms BG, Lee CW, Aumuller G, Seitz J. Instructive induction of prostate growth and differentiation by a defined urogenital sinus mesenchyme. Microsc Res Tech 1995; 30:319–332.
33. Cunha GR. Age-dependent loss of sensitivity of female urogenital sinus to androgenic conditions as a function of the epithelia-stromal interaction in mice. Endocrinology 1975; 97:665–673.
34. Thomson AA, Timms BG, Barton L, Cunha GR, Grace OC. The role of smooth muscle in regulating prostatic induction. Development 2002; 129: 1905–1912.
35. Takayanagi S, Tokunaga T, Liu X, Okada H, Matsushima A, Shimohigashi Y. Endocrine disruptor bisphenol A strongly binds to human estrogen-related receptor gamma (ERRgamma) with high constitutive activity. Toxicol Lett 2006; 167:95–105.
36. Susens U, Hermans-Borgmeyer I, Borgmeyer U. Alternative splicing and expression of the mouse estrogen receptor-related receptor gamma. Biochem Biophys Res Commun 2000; 267:532–535.
37. Nakanishi T, Kohroki J, Suzuki S, Ishizaki J, Hiromori Y, Takasuga S, Itoh N, Watanabe Y, Utoguchi N, Tanaka K. Trialkyltin compounds enhance human CG secretion and aromatase activity in human placental choriocarcinoma cells. J Clin Endocrinol Metab 2002; 87:2830–2837.
38. Horiguchi T. Masculinization of female gastropod mollusks induced by organotin compounds, focusing on mechanism of actions of tributyltin and triphenyltin for development of imposex. Environ Sci 2006; 13:77–87.
39. Cunha GR, Donjacour A. Stromal-epithelial interactions in normal and abnormal prostatic development. Prog Clin Biol Res 1987; 239:251–272.
40. Richter CA, Taylor JA, Ruhlen RL, Welshons WV, Vom Saal FS. Estradiol and bisphenol A stimulate androgen receptor and estrogen receptor gene expression in fetal mouse prostate mesenchyme cells. Environ Health Perspect 2007; 115:902–908.
41. Ricke WA, McPherson SJ, Bianco JJ, Cunha GR, Wang Y, Risbridger GP. Prostatic hormonal carcinogenesis is mediated by in situ estrogen production and estrogen receptor alpha signaling. FASEB J 2008; 22: 1512–1520.

毒性学

Percellomeトキシコゲノミクスの進捗

Progress in percellome toxicogenomics

Percellomeトキシコゲノミクスプロジェクトとは

2006年に本誌の当欄にて，毒性学の高精度解析手法として開始した“Percellomeトキシコゲノミクスプロジェクト”を紹介させていただいた[1]．当毒性部の基本姿勢は変わらず，さまざまな物質が身体に取り込まれた際に生じる可能性のある毒性(有害性)を予測し，それらの使用に際しての被害を未然に防ぐのが毒性学の役割であるとの考えに立脚し，身のまわりにあり，体のなかに入ってくるすべての“もの”について，どのような場合に(胎児・新生児・小児など，吸い込む・飲み込むなど)，どのくらいの量で，どのような症状が現れるか(急性毒性，発癌を含む慢性毒性，遅発性毒性など)について研究を継続している．

具体的には実験動物の診断所見をヒトに外挿すべく実施しているが，従来法では種差や個体差は“安全係数”により量的な安全マージンをとることで勘案されてきた．しかし，サリドマイド奇形に代表されるように，これには科学的な限界があり，“毒性学の近代化”が必要である．医薬品の場合はヒトで治験を行える場合があるが，それも胎児や新生児には実施困難であり，一般的な物質の毒性を検討することを考えると現状では動物実験は不可避である．そこで，著者らはヒトの身代りとしての実験動物(遺伝子改変動物の活用を含む)を対象とした，Percellomeトキシコゲノミクス研究を開始した次第である．

これは生体というブラックボックスの中身を遺伝子発現ネットワークの面から解明することにより，生体反応メカニズムに基づいた分子毒性学を構築することを目的としている．その際，毒性を見落とさない“網羅性”を確保する必要性から，全遺伝子のトランスクリプトーム情報のなかから生物学的に有意と判断される反応ネットワークを網羅的に抽出するアプローチをとっている．複数の実験から得られる大量のデータを蓄積し横断的な解析を加えることが必須であることから，マイクロアレイデータの標準化と互換性確保のために“細胞1個当りのmRNAコピー数”を得るPercellome法[2]を開発し，プロジェクトを軌道に乗せたところまでを前回の記事でご紹介した．

最近の展開

その後の数年間に，100種類超(医薬品，一般化学物質，食品関連物質を含む)の化学物質によるマウス肝の初期応答データを含む，延べ3.5億遺伝子情報からなるPercellomeデータベースを得た．これは，基本的に投与後の時間，曝露用量，遺伝子発現量の3軸からなる三次元曲面データにより構成される(図1)．解析には，この三次元曲面の特徴抽出という独創的な方法をとり，解析ソフトウェア群(相崎健一ら)は独自開発である．また，動物実験レベルからのシステム管理により，高精細かつ高再現性を実現している．

得られたデータの例としては，アリル炭化水素受容体(AhR)に結合するダイオキシン(2，3，7，8-TCDD)が比較的少数のAhR直下の遺伝子の発現を2時間目に誘導し，4，8，24と時間が経過する

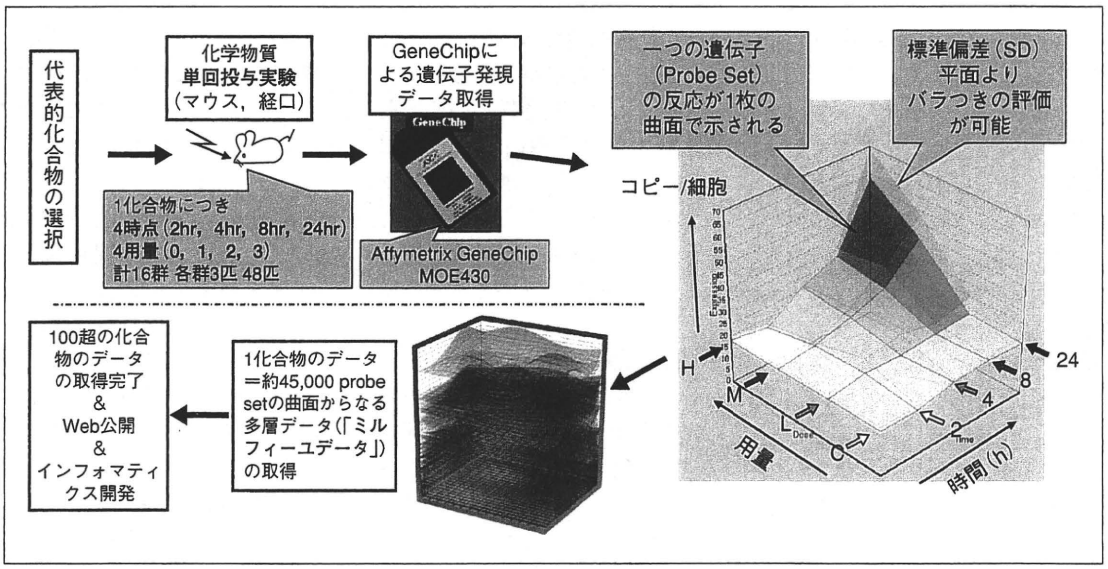

図1　Percellomeデータベースの概要

につれ数を増す状況が確認された．ダイオキシンの体内半減期が25時間であるにもかかわらず，2時間目のみの一過性発現のパターンをとるもの，持続的に発現が増加するものなどが観測されている．シックハウス症候群の指針値程度の，ごく低濃度域での吸入毒性トキシコゲノミクスも実施しており，ごく低濃度のホルマリン(0.1 ppm 付近)で肺の複数の遺伝子発現が明確に誘導されることをみている．サリドマイドは近年，癌治療薬として使用されていることから，複数の臓器における初期誘導を観測したところ，肺の2時間目に用量相関性をもって発現誘導のピークを示す遺伝子に，Cdkn1a (P21)が認められた．類似の発現パターンを示す初期応答遺伝子には，Fas，Foxo3a，Gata2など50あまりがあり，酸化的ストレスが誘発されることが推測された．実際，癌患者にサリドマイドが間質性肺炎を誘発する報告が増加しており，ヒトで確認された形となっている．

また，Percellomeトキシコゲノミクスを発生毒性へも適用している．妊娠マウスにサリドマイドを投与し胎児で発現変動が認められた遺伝子のなかに，マウス胚の肢部形成に重要な分子が見出され(その遺伝子をノックアウトしたマウス胚にアザラシ肢症に類似の奇形が生じる)，サリドマイド奇形の標的分子検索の糸口が示唆された．さらに，胎生期～幼若期の発達中の脳に対する神経シグナル撹乱が脳構造や神経回路の形成に影響を及ぼし，成熟後に行動異常などの脳高次機能の障害として顕在化することを見出している．これについては，妊娠マウスへ神経伝達物質類似物質を投与し，生まれたマウスに誘発される遅発性中枢毒性と海馬の遺伝子発現異常の関連解析から標的ネットワークが示唆されつつある．

このほかにも投与した化学物質に関して，いままで報告のないあらたな遺伝子発現変動現象を多数見出し，そのいくつかには特定の毒性との連鎖を示唆する分子生物学的情報がみつかっていることから，それらを順次報告および一般公開する準備を進めている(http://www.nihs.go.jp/tox/TTG_Archive.htm；現在更新中．2010年度中再開予定)．

プロジェクトの今後

さらに，マイクロアレイのクロスハイブリダイゼーションを修正するアルゴリズムの開発を終え(特許出願準備中)，その実装準備中である(NTTデータおよび日本テラデータとの委託共同研究)．また，遺伝子ネットワークと毒性の動的な因果関係を導き出すインフォマティクスの構築研究やPercellomeデータの統合的提示方法の開発にも本格的に取り組んでおり(ソニーコンピュータサイエンス研究所との共同研究)，段階的に皆様にご披露できる予定である(厚生労働科学研究費補助金，環境研究総合推進費などによる)．

1) 菅野　純：毒性の高精細解析に向けてのトキシコゲノミクス．医学のあゆみ，**218**：1035-1036，2006．
2) Kanno, J. et al.："Per cell" normalization method for mRNA measurement by quantitative PCR and microarrays. *BMC Genomics*, **7**：64, 2006.

菅野　純／Jun KANNO
国立医薬品食品衛生研究所
安全性生物試験研究センター毒性部

循環器内科学

心筋トロポニンの高感度測定の有用性

Clinical utility of high-sensitivity cardiac troponin assay

従来の心筋トロポニン測定は検出感度が低いため，急性冠症候群の診療以外で用いられることはまれであった．最近，検出感度が5倍以上改善された高感度測定が臨床の場に登場した．この高感度測定は，従来測定では検出不可能であった小さな心筋障害を診断できる．そのため，超急性期の心筋梗塞診断の精度[1,2]や慢性心不全における予後予測の精度[3]を高めることが示されている．さらに，外来診療や検診・人間ドック分野へのあらたな展開も期待される．

急性冠症候群の診療

トロポニンが上昇している不安定狭心症は，突然死や急性心筋梗塞発症の危険度が高い．このトロポニンの上昇は，破砕したプラークや血栓が引き起した末梢の微小塞栓による微小心筋障害を反映している．そのため，2000年に公表されたヨーロッパ心臓病学会/アメリカ心臓病学会(ESC/ACC)の心筋梗塞の再定義[4]は，トロポニンが上昇している不安定狭心症を急性心筋梗塞に包括した．さらに，ヨーロッパ心臓病学会/アメリカ心臓病学会/アメリカ心臓協会/世界心臓協会(ESC/ACC/AHA/WHF)の共同タスクフォースは，2007年に急性心筋梗塞の診断基準の再改定[5]を公表した．新しい診断基準では，トロポニンの心筋梗塞診断における基準値を健常人の99thパーセンタイル値より大と定めた．一般に，測定値の相対的なばらつき(変動係数．coefficient of variation：CV)が小さいほど測定値の精度は高い．共同タスクフォースは試薬の精度にも言及しており，健常人の99thパーセンタイル値における変動係数が10%以下である試薬を用いることを推奨した．従来の試薬はこの条件を

Development 137, 1515-1522 (2010) doi:10.1242/dev.044545

The oscillation of Notch activation, but not its boundary, is required for somite border formation and rostral-caudal patterning within a somite

Masayuki Oginuma[1,2,*], Yu Takahashi[3,*], Satoshi Kitajima[3], Makoto Kiso[2], Jun Kanno[3], Akatsuki Kimura[1,4] and Yumiko Saga[1,2,†]

SUMMARY

Notch signaling exerts multiple roles during different steps of mouse somitogenesis. We have previously shown that segmental boundaries are formed at the interface of the Notch activity boundary, suggesting the importance of the Notch on/off state for boundary formation. However, a recent study has shown that mouse embryos expressing Notch-intracellular domain (NICD) throughout the presomitic mesoderm (PSM) can still form more than ten somites, indicating that the NICD on/off state is dispensable for boundary formation. To clarify this discrepancy in our current study, we created a transgenic mouse lacking NICD boundaries in the anterior PSM but retaining Notch signal oscillation in the posterior PSM by manipulating the expression pattern of a Notch modulator, lunatic fringe. In this mouse, clearly segmented somites are continuously generated, indicating that the NICD on/off state is unnecessary for somite boundary formation. Surprisingly, this mouse also showed a normal rostral-caudal compartment within a somite, conferred by a normal Mesp2 expression pattern with a rostral-caudal gradient. To explore the establishment of normal Mesp2 expression, we performed computer simulations, which revealed that oscillating Notch signaling induces not only the periodic activation of *Mesp2* but also a rostral-caudal gradient of Mesp2 in the absence of striped Notch activity in the anterior PSM. In conclusion, we propose a novel function of Notch signaling, in which a progressive oscillating wave of Notch activity is translated into the rostral-caudal polarity of a somite by regulating *Mesp2* expression in the anterior PSM. This indicates that the initial somite pattern can be defined as a direct output of the segmentation clock.

KEY WORDS: Notch signaling, Hes7, Mesp2, Segmentation clock, Presomitic mesoderm, Lunatic fringe, Somitogenesis

INTRODUCTION

The periodicity of the segmented somites is established in the posterior presomitic mesoderm (PSM) via the function of a so-called molecular clock, which is based on complex gene regulatory networks under the control of three major signaling pathways: Notch, Fgf and Wnt (Dequeant et al., 2006; Dequeant and Pourquie, 2008). Among these pathways, Fgf and Wnt are implicated in the maintenance of immature PSM cells (Aulehla et al., 2003; Aulehla et al., 2008; Wahl et al., 2007; Delfini et al., 2005; Niwa et al., 2007), whereas Notch signaling might be directly involved in the generation of periodicity (Oginuma et al., 2008; Yasuhiko et al., 2006; Takahashi et al., 2000; Takahashi et al., 2003). In mice, Notch signal oscillations are produced by the suppressive function of the glycosyltransferase lunatic fringe (Lfng) as the levels of activated Notch1 (cleaved form of the Notch1 intracellular domain, referred to as cNICD hereafter) are upregulated in the *Lfng*-null mouse embryo (Morimoto et al., 2005). The expression of *Lfng* exhibits a biphasic pattern involving oscillation in the posterior PSM and a stabilized striped pattern in the anterior PSM (Aulehla and Johnson, 1999; McGrew et al., 1998; Morales et al., 2002; Cole et al., 2002). The oscillatory expression of *Lfng* is positively regulated by Notch signaling as it is greatly downregulated in *Dll1*-null mice, whereas it is negatively regulated by Hes7 as revealed by its upregulation in *Hes7*-null embryos (Barrantes et al., 1999; Bessho et al., 2003; Morales et al., 2002). The stabilized expression of *Lfng* is under the control of the Mesp2 transcription factor and stabilization does not occur in the absence of Mesp2 (Morimoto et al., 2005). In the absence of Lfng, no clear segmental border is defined and the rostral-caudal (R-C) compartmentalization within a somite is randomized (Zhang and Gridley, 1998; Evrard et al., 1998).

In the anterior PSM, the Mesp2 transcription factor plays an important role in the creation of a cNICD on/off state that corresponds to the future segmental boundary via the activation of Lfng transcription (Morimoto et al., 2005). This suggests that the Notch on/off state is important for boundary formation. However, a recent study has shown that mouse embryos expressing Notch activity throughout the PSM still show the ability to form more than ten somites, indicating that the Notch on/off state is dispensable for boundary formation (Feller et al., 2008). By contrast, however, other studies have reported that transgenic mice expressing *Lfng* only in the anterior PSM show normal segmental border formation after embryonic day 10.5 (E10.5), suggesting that the Notch on-off state generated in the anterior PSM is sufficient to create a somite boundary at least in the later stage embryos (Shifley et al., 2008; Stauber et al., 2009).

To resolve this discrepancy, we have, in our current study, generated a mouse that lacks the anterior striped Lfng expression pattern, but at the same time retains oscillating Lfng activity in the

[1]Department of Genetics, SOKENDAI, 1111 Yata, Mishima, Shizuoka 411-8540, Japan. [2]Division of Mammalian Development, National Institute of Genetics, Yata 1111, Mishima 411-8540, Japan. [3]Division of Cellular and Molecular Toxicology, National Institute of Health Sciences, 1-18-1 Kamiyoga, Setagaya-ku, Tokyo 158-8501, Japan. [4]Cell Architecture Laboratory, National Institute of Genetics, Yata 1111, Mishima 411-8540, Japan.

*These authors contributed equally to this work
†Author for correspondence (ysaga@lab.nig.ac.jp)

Accepted 17 February 2010

posterior PSM. The resulting transgenic mouse shows no clear cNICD on/off state in the anterior PSM. Nevertheless, this mouse exhibits normal boundary formation, indicating that the cNICD boundary is dispensable for somite formation. In addition, our transgenic mouse shows normal R-C patterning within a somite. Further analyses by computer simulation have led us to conclude that Notch signaling oscillation functions as an output signal that is both required and sufficient to establish the *Mesp2* expression pattern needed for normal somitogenesis.

MATERIALS AND METHODS

Animals

The wild-type mice used in this study were the MCH strain (a closed colony established at CLEA, Japan). The *Lfng*-null (Evrard et al., 1998), *Mesp2*-null (*Mesp2*$^{MCM/+}$) (Takahashi et al., 2007) and *Mesp2-lacZ* (*Mesp2*$^{lacZ/+}$) (Takahashi et al., 2000) mouse lines are maintained in the animal facility of the National Institute of Genetics and National Institute of Health Sciences, Japan.

Gene targeting strategy to generate the *Mesp2*^{Lfng} allele

The knock-in strategy used to target the *Mesp2* locus is largely similar to our previously described method (Takahashi et al., 2000), except that *Lfng* cDNA was inserted. The *pgk-neo* cassette flanked by a *lox* sequence was removed by crossing with *CAG-Cre* mice (Sakai and Miyazaki, 1997).

Generation of the *Hes7-Lfng* transgenic mice

We used a 12 kb *Hes7* gene cassette comprising 5 kb of upstream sequence and all of the exons and introns, as this construct had previously been confirmed to be sufficient to reproduce the endogenous *Hes7* oscillation pattern when inserted in-frame at the translational start site (Kageyama et al., personal communications). We generated the construct *Lfng IRES-EGFP*, in which *IRES* (internal ribosomal entry site)-*EGFP* (enhanced GFP) was fused to the 3′ end of *Lfng* cDNA, and inserted this construct into the *Hes7*-translational initiation site. The resulting DNA was digested with restriction enzymes to remove vector sequences and gel purified. Transgenic mice were generated by microinjection of this construct into fertilized eggs, which were then transferred into the oviducts of pseudopregnant foster females.

In situ hybridization, immunohistochemistry, histology and skeletal preparations

The methods used for wholemount in situ hybridization, section in situ hybridization, immunohistochemistry, histology and skeletal preparation by Alcian Blue/Alizarin Red staining are described in our previous reports (Morimoto et al., 2005; Oginuma et al., 2008; Takahashi et al., 2000). The cNICD signal was detected by immunohistochemistry using anti-cleaved NICD (Val1744; 1:500; Cell Signaling Technology). Probes were prepared also as described previously: *Mesp2* exon-intron (Oginuma et al., 2008), *Mesp2* (Takahashi et al., 2000) and *Lfng* (Evrard et al., 1998). The *GFP* cRNA probe was prepared by PCR-amplification of *GFP* cDNA.

Computer simulation

Our computer simulation model is based on the previous mathematical description of a clock-and-wavefront model constructed by J. Lewis (Palmeirim et al., 1997). By using the basic oscillating function in the Lewis model, we modeled the activity of cNICD, n, at given time, t, and anteroposterior position, x, as:

$$n(x,t)=\left[1-\cos\left\{2\pi\int_0^t\frac{1}{1+e^{(x+t)/2}}dt\right\}\right]/2\,.$$

For the control simulation with constant activity of cNICD, the cNICD activity, n, was set to 0.3. For the simulation with oscillating cNICD without wave, n was formulated as $n(x,t)=\{1-\cos(\pi t)\}/2$. The activity of Fgf8 is known to gradually decrease from posterior to anterior, and also according to the time elapsed. These features of Fgf8 fit well with the formulation of the clock cycling rate in the Lewis model and, thus, we calculated the activity of Fgf8, f, using the formula $f(x,t)=1/(1+e^{(x+t)/2})$.

We next added the regulation of Mesp2 and Tbx6 expression to the model. As cNICD and Fgf8 play positive and negative roles for *Mesp2* expression, respectively, we assumed that the increase of *Mesp2* expression occurs when the cNICD activity, n, exceeds that of Fgf8, f, with the amount dependent on n–f. Tbx6 (b) is also required for *Mesp2* expression. We thus modeled the *Mesp2* mRNA expression, m, and Mesp2 protein expression, p, as:

$$m(x,t+\Delta t)=m(x,t)+S_m\times\frac{[\{n(x,t)-f(x,t)\}/K_n]^{H_n}}{1+[\{n(x,t)-f(x,t)\}/K_n]^{H_n}}\times\frac{\{b(x,t)/K_b\}^{H_b}}{1+\{b(x,t)/K_b\}^{H_b}}-D_m\times m(x,t)\,,$$

$$p(x,t+\Delta t)=p(x,t)+S_p\times m(x,t-T)-D_p\times p(x,t)\,,$$

with the initial condition $m(x,0)=0$, and $p(x,0)=0$. The degradation of Tbx6 is dependent on Mesp2 (Oginuma et al., 2008). We introduced a hypothetical molecule, z, that is expressed depending on Mesp2 and degrades Tbx6 by interacting with it. The expression of Tbx6 (b) and the Tbx6 degrading molecule (z) were modeled as:

$$z(x,t+\Delta t)=z(x,t)+S_z\times\frac{\{p(x,t-T)/K_p\}^{H_p}}{1+\{p(x,t-T)/K_p\}^{H_p}}-D_z\times z(x,t)\,,$$

$$b(x,t+\Delta t)=b(x,t)-D_b\times\{b(x,t)\}^{Bb}\times\{z(x,t)\}^{Bz}\,,$$

with the initial condition $z(x,0)=0$, and $b(x,0)=1.0$.

These formulas were implemented using C language. The activities of cNICD (n), Fgf8 (f), Mesp2 (m and p), Tbx6-regulator (z) and Tbx6 (b) were calculated over the ranges $-12.5\leq x\leq -2.5$ and $0\leq t\leq 20$. The calculations were conducted discretely with a single unit of x (Δx) of 1/10 and t (Δt) of 1/10. The parameter values we used are shown in Table S1 in the supplementary material. We also introduced time delay, $T=2\Delta t$, for protein expression (Lewis, 2003), which did not affect the results much.

RESULTS

Dissection of the *Lfng* expression pattern in the PSM

To examine the significance of the Notch on/off state during boundary formation, we focused on *Lfng* expression, which exhibits a biphasic pattern involving oscillation in the posterior PSM and a stabilized striped pattern in the anterior PSM (Aulehla and Johnson, 1999; Cole et al., 2002; McGrew et al., 1998; Morales et al., 2002). Each of these two patterns is implicated in the generation of the corresponding Notch activity profile via negative regulation. To induce only the oscillatory expression of *Lfng*, we utilized the *Hes7* transcriptional regulatory unit as the oscillation of *Lfng* and *Hes7* is regulated by similar factors, i.e. positively by Notch signaling and negatively by Hes7 protein. As shown in Fig. 1, these two transcripts show similar expression patterns in the oscillation phase. Both signals manifest a waved pattern within the Tbx6 expression domain from phase I to phase III (Fig. 1A-L). However, in phases I-II, *Hes7* expression is lost from the anterior domain (Fig. 1G-J), whereas that of *Lfng* persists for a longer period in the anterior PSM and forms a clear stripe (Fig. 1A-D,M,O). It should also be noted that the anterior *Lfng* expression domain was found to merge with that of the Mesp2 protein (Fig. 1N,P), the expression of which is restricted to the anterior PSM. This is not unexpected as *Lfng* expression is induced by Mesp2 in the anterior PSM and creates the Notch on/off state (Morimoto et al., 2005). Taken together, we concluded from these data that the *Lfng* expression pattern can be reproduced by two distinct regulatory systems – the *Hes7* promoter-enhancer and the *Mesp2* regulatory system – and this enabled us to further investigate the significance of Notch activities.

The cNICD on/off state is not required for somite boundary formation

To further elucidate the functional significance of the oscillatory cNICD in the posterior PSM and that of the cNICD on/off state in the anterior PSM, we generated a transgenic mouse line by inserting *Lfng* cDNA flanked with *IRES-EGFP* under the control of the Hes7 promoter (see Fig. S1A in the supplementary material). As expected, the expression pattern of this transgene, examined by in situ hybridization using *EGFP* as a probe, was found to be very similar to that of endogenous *Hes7* and *Lfng* except for the lack of anterior striped expression (see Fig. S1B-D in the supplementary material). We then introduced this transgene into the *Lfng*-null genetic background to establish the *Hes7>Lfng/Lfng*$^{-/-}$ mouse line and examined the expression pattern of exogenous *Lfng* and cNICD expression in the absence of endogenous *Lfng* expression (i.e. an *Lfng*-null background). In wild-type embryos, *Lfng* and cNICD showed biphasic patterns, these being oscillation in the posterior PSM and stabilization in the anterior PSM, whereas cNICD oscillation was barely detectable and a constant level of cNICD could be observed through the entire PSM in the absence of *Lfng*, as reported previously (Morimoto et al., 2005). In the *Hes7>Lfng/Lfng*$^{-/-}$ embryo, however, we observed the recovery of cNICD oscillation in the posterior PSM, which overlapped with *Lfng* expression (Fig. 2A-F), clearly indicating that the *Lfng* transgene was functionally active in these embryos. In addition, we previously showed that cNICD and Mesp2 generate a clear boundary in the anterior PSM, which demarcates the presumptive segmental border in phase-II embryos (Morimoto et al., 2005) (Fig. 2G-I). In the absence of *Lfng*, this clear border between cNICD and Mesp2 was not generated and a merged pattern was instead observed

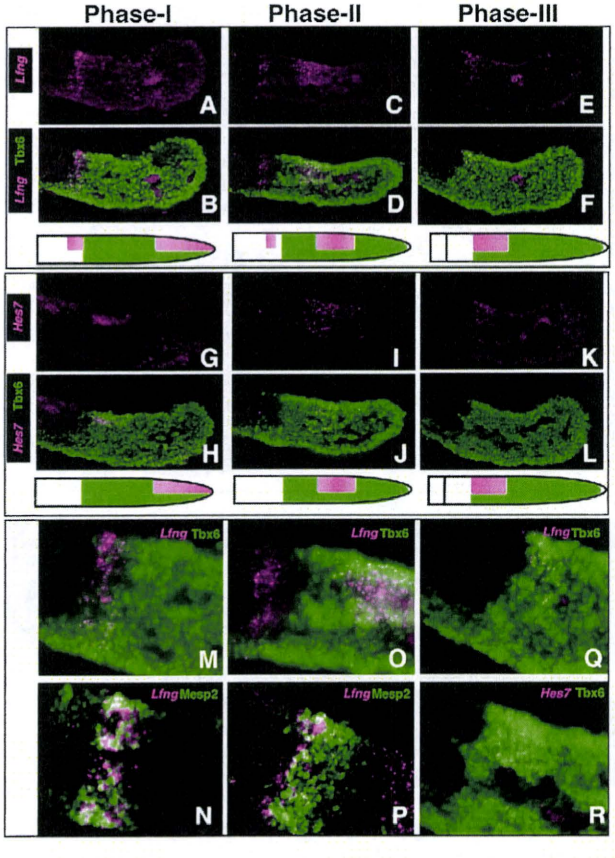

Fig. 1. Comparison of the *Hes7* and *Lfng* expression patterns. In situ hybridization analysis of the spatiotemporal changes in the *Lfng* (**A-F**) and *Hes7* (**G-L**) transcription patterns during somitogenesis by double staining for the Tbx6 protein as the reference point. The stained sections shown in the vertical rows are derived from a single embryo. The phase was defined by the location of the *Hes7* and *Lfng* transcripts and the waves of oscillating *Hes7* and *Lfng* were initiated at the posterior PSM (Phase I). The oscillating wave then moves to the intermediate PSM (Phase II) and reaches the anterior PSM (Phase III). (**M**,**O**,**Q**,**R**) Magnified images of B, D, F and L, respectively. Phase I and Phase II sections were also subjected to double staining for *Lfng* mRNA and Mesp2 (**N**,**P**).

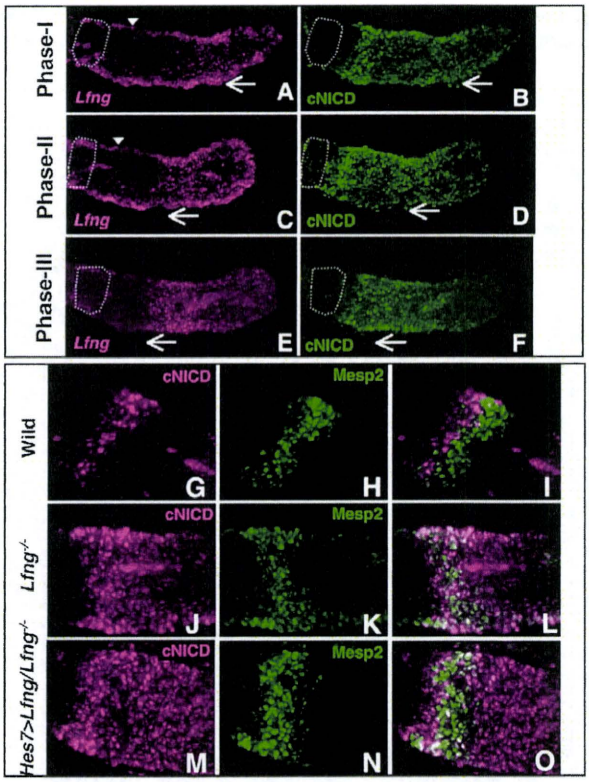

Fig. 2. *Hes7>Lfng/Lfng*$^{-/-}$ mice show cNICD oscillation in the posterior PSM but do not form a cNICD boundary in the anterior PSM. (**A-F**) The patterns of *Lfng* mRNA (A,C,E) and cNICD (B,D,F) expression were revealed in each channel by double staining of these signals using single embryos of *Hes7>Lfng/Lfng*$^{-/-}$ mice at three different phases, I-III, respectively. *Lfng* expression shows a traveling wave (arrow) but no stabilized stripe (arrowheads, A,C). The first somite is indicated by a white dotted line. The wave of oscillating cNICD is initiated at the posterior PSM (B; Phase I; *n*=3), moves to the intermediate PSM (D; Phase II; *n*=4) and eventually reaches the anterior PSM (F; Phase III; *n*=3). (**G-O**) The relationship between cNICD and Mesp2 in Phase II was compared among wild-type (G-I), *Lfng*$^{-/-}$ (J-L) and *Hes7>Lfng/Lfng*$^{-/-}$ (M-O) embryos by double staining. Single channels for cNICD (G,J,M) and Mesp2 (H,K,N), and merged images of both (I,L,O), are shown. In the wild-type embryos, cNICD and Mesp2 generate a clear boundary (I). *Lfng*$^{-/-}$ and *Hes7>Lfng/Lfng*$^{-/-}$ mice, however, do not show a clear segregation between cNICD and Mesp2 (L,O).

(Fig. 2J-L). In the *Hes7>Lfng/Lfng*$^{-/-}$ embryo, as expected by the lack of Lfng expression in the anterior PSM, we did not detect segregation between the cNICD and Mesp2 domains (Fig. 2M-O). *Lfng*$^{-/-}$ embryos did not show clear somite boundaries, although incomplete somites did appear to be formed (see Fig. S2 in the supplementary material), as also suggested previously (Evrard et al., 1998; Zhang and Gridley, 1998). Very surprisingly, however, *Hes7>Lfng/Lfng*$^{-/-}$ embryos showed clearly segmented somites (Fig. 3A-C). This strongly indicates that the oscillatory expression of cNICD mediated via oscillating Lfng is sufficient to provide the conditions for normal somitogenesis to occur and that the cNICD boundary in the anterior PSM is not required for this process.

Recently, we and others have suggested that the Mesp2 downstream events, such as the activation of ephrin-EphA4 signaling and the formation of a Tbx6 protein boundary, were more important for segmental border formation (Watanabe et al., 2009; Oginuma et al., 2008; Nakajima et al., 2006). In *Lfng*$^{-/-}$ embryos, the expression of *EphA4* and the Tbx6 protein boundary were found to be diffuse or randomized (Fig. 3E,J-L), whereas in *Hes7>Lfng/Lfng*$^{-/-}$ embryos, these expression patterns appeared to be normal (Fig. 3F,M-O), i.e. similar to those in wild-type embryos (Fig. 3D,G-I). Taken together, our current findings show that the cNICD boundary is dispensable, but that the Mesp2 boundary might be required, for the creation of the segmental border through the regulation of downstream genes.

R-C polarity is completely recovered in *Hes7>Lfng/Lfng*$^{-/-}$ embryos

We next further examined the morphological features of the *Hes7>Lfng/Lfng*$^{-/-}$ embryo. Surprisingly, these transgenic embryos showed a completely normal skeletal system, with segmented vertebra and ribs (Fig. 4A-C). Furthermore, the expression pattern of *Uncx4.1*, a caudal marker of R-C polarity (Fig. 4D), was fully recovered in the *Hes7>Lfng/Lfng*$^{-/-}$ embryo (Fig. 4F), which contrasts with the randomized pattern we observed in the *Lfng*$^{-/-}$ embryo (Fig. 4E). These results suggest that the cNICD boundary in

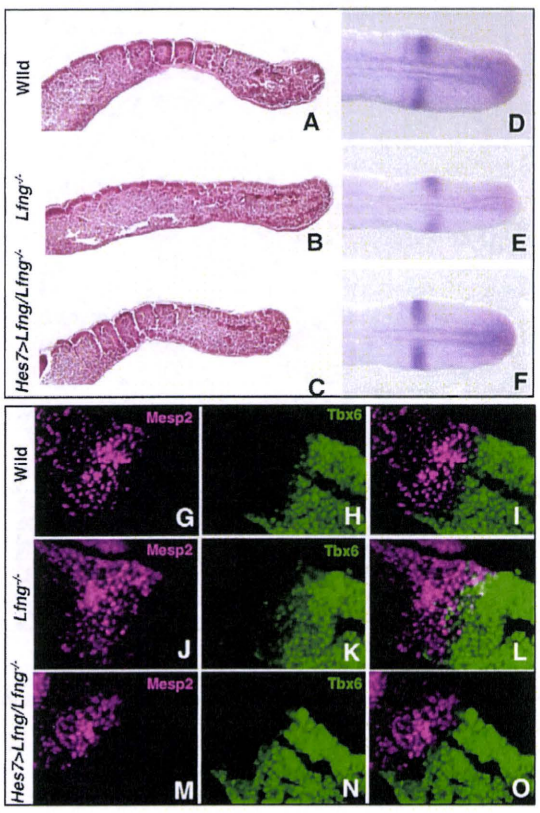

Fig. 3. Exogenous *Lfng* controlled by the *Hes7* promoter completely rescues the boundary formation defect in the *Lfng*$^{-/-}$ mice. The segmental morphologies (**A-C**), the *EphA4* expression pattern (**D-F**) and the relationship between Mesp2 and Tbx6 in Phase II (**G-O**) were compared among wild-type (A,D,G-I), *Lfng*$^{-/-}$ (B,E,J-L) and *Hes7>Lfng/Lfng*$^{-/-}$ (C,F,M-O) using E11.5 embryonic tail regions. Single channels for Mesp2 (G,J,M) and Tbx6 (H,K,N), and merged images of both (I,L,O), are shown. Expression of the *EphA4* and Tbx6 protein boundary forms a clear border in the wild-type (D, *n*=7; G-I, *n*=4) and *Hes7>Lfng/Lfng*$^{-/-}$ embryos (F, *n*=4; M-O, *n*=4), but this is diffuse or randomized in the *Lfng*$^{-/-}$ embryos (E, *n*=4; J-L, *n*=3).

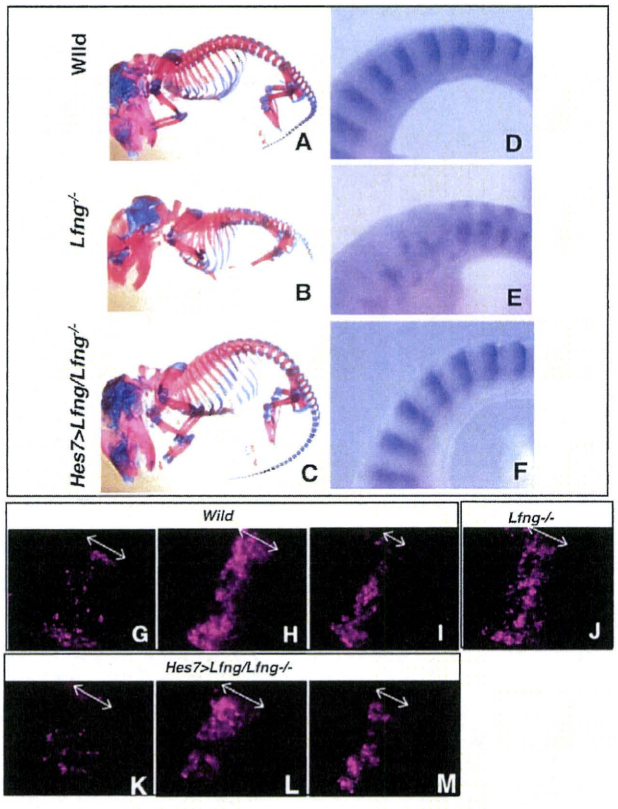

Fig. 4. Exogenous *Lfng* under the control of the *Hes7* promoter completely rescues the R-C patterning defect in the somites of *Lfng*$^{-/-}$ mice. A comparison of the segmental morphologies of skeletal preparations of E17.5 embryos (**A-C**) and the expression pattern of *Uncx4.1*, indicative of R-C patterning within a somite (**D-F**). *Hes7>Lfng/Lfng*$^{-/-}$ mice show a normal skeleton (C, *n*=4) and expression pattern of *Uncx4.1* (F, *n*=3), whereas *Lfng*$^{-/-}$ mice show randomized pattern of skeleton (B) and *Uncx4.1* expression (E). (**G-M**) *Mesp2* transcription states revealed by high resolution in situ hybridization analysis of wild-type embryos for transcriptional initiation (G, *n*=3), active state (H, *n*=5) and rostral localization (I, *n*=3), and *Lfng*-null (J, *n*=11) and *Hes7>Lfng/Lfng*$^{-/-}$ embryos for transcriptional initiation (K, *n*=2), active state (L, *n*=3) and rostral localization (M, *n*=3). Double arrows indicate the length of the *Mesp2* transcription domains.

the anterior PSM is not required for normal R-C polarity patterning. To elucidate this issue further, we focused on the expression of *Mesp2*, which is thought to be the final output signal of the segmentation clock. *Mesp2* is initially expressed over one somite length and then becomes localized in the rostral compartment (Takahashi et al., 2000). This dynamic expression pattern generates a gradient of Mesp2 activity that allows PSM cells to form the R-C pattern within a somite (Takahashi et al., 2003; Takahashi et al., 2000). We therefore next compared the *Mesp2* expression pattern at the cellular level among the wild-type, $Lfng^{-/-}$ and $Hes7>Lfng/Lfng^{-/-}$ embryos using high-resolution in situ hybridization. By focusing on the length of the *Mesp2* transcription domain along the A-P axis, we found four distinct patterns in the wild-type embryos: (1) no signal (n=4/15); (2) most cells show nuclear dots indicating transcriptional initiation, and the length of the *Mesp2* transcription domain is approximately 11-13 cells (Fig. 4G; n=3/15); (3) active stage in which signals can be observed in the cytoplasm in addition to nuclear dots, and the length of *Mesp2* transcription is approximately 10-12 cells, with anterior cells showing stronger signals (Fig. 4H; n=5/15); and (4) rostral localization in which the length of the *Mesp2* transcription domain becomes approximately 5-6 cells (Fig. 4I; n=3/15). In contrast to wild-type embryos, only one pattern was observed in the *Lfng*-null embryos: signals were observed in the cytoplasm in addition to nuclear dots, the expression levels were randomized for each cells, and the length of the *Mesp2* transcription domain was approximately 9-11 cells (Fig. 4J; n=11/11). These results indicate that *Mesp2* expression is always present in the anterior PSM without clear on/off cycles in the *Lfng*-null embryo. In addition, the *Mesp2* expression domain is kept to one somite length and there is no clear localization into the rostral compartment, although cellular or cell cluster-level localization might occur in a salt-and-pepper pattern in the absence of Lfng. Importantly, the *Mesp2* expression pattern was found to show four distinct patterns similar to those in wild-type embryos even in the $Hes7>Lfng/Lfng^{-/-}$ embryos, i.e. no signal (1/9), transcriptional initiation (Fig. 4K, n=2/9), active stage (Fig. 4L, n=3/9) and rostral localization (Fig. 4M; n=3/9). Our findings thus indicate that the oscillation of cNICD alone is sufficient to generate the normal *Mesp2* expression pattern and that the anterior PSM-specific regulation of cNICD via Lfng is dispensable for this process.

Modeling of the *Mesp2* expression pattern

To test the validity of our above hypothesis, we performed computer simulations. Our model is based on that previously proposed by Lewis and colleagues, in which the oscillatory waves emanate, travel and eventually cease, as it adopts the notion of maturity, which delays the oscillation cycle towards the anterior as time proceeds (Palmeirim et al., 1997). In this model of Lewis, the cessation of the oscillatory waves triggers periodic gene expression along an anterior-posterior direction that leads to the formation of the somites (Palmeirim et al., 1997). In our current study, we applied the Lewis model to the oscillatory waves of the cNICD and assumed Fgf as a molecular basis for maturity. We further incorporated the regulatory network required for *Mesp2* expression, in which cNICD oscillation and Tbx6 synergistically activate (Yasuhiko et al., 2006; Oginuma et al., 2008), whereas the Fgf gradient suppresses *Mesp2* expression and Tbx6 is degraded downstream of Mesp2 (Fig. 5A). Very surprisingly, this simple simulation successfully mimicked some specific features of dynamic *Mesp2* transcription (red line), not only in terms of on/off cycles but also with regard to temporal changes in the expression pattern (from one somite length to rostral localization) along the anterior-posterior axis (Fig. 5B; see Movie 1 in the supplementary material), similar to that observed in vivo (Fig. 4G-I; see Fig. S3A,B in the supplementary material). In addition, this simulation also reproduced the gradient of Mesp2 activity accumulation (black line), which is similar to the *Mesp2*-β-gal pattern we observed in the $Mesp2^{lacZ/+}$ embryos (see Fig. S3E in the supplementary material).

To test the importance of the cNICD wave for the gradient formation of Mesp2 activity, we examined *Mesp2* expression under constant activity of cNICD in the PSM (Fig. 5C; see Movie 2 in the supplementary material). In this instance, *Mesp2* expression is always observed in the anterior PSM without either clear on/off cycles or localization at the rostral compartment, which is very similar to the in vivo situation of the $Lfng^{-/-}$ embryos (Fig. 4J; see Fig. S3C,D,F in the supplementary material). Interestingly, in our model, neither the formation of the waved pattern of cNICD nor its migration is necessary to establish the gradient of Mesp2 activity because a spatially uniform, but temporally oscillating, Notch signaling activity is sufficient to reproduce this gradient (see Fig. S4 and Movie 3 in the supplementary material). Without a traveling wave, however, the temporal transition of the Mesp2 expression pattern from a one-somite length to a rostral localization was not reproduced (see Fig. S4 and Movie 3 in the supplementary material). We thus speculate that this transition might be important for robust somite formation with a correct R-C polarity and propose that the wave of Notch activity enables PSM cells to establish not only the periodic expression of *Mesp2*, but also their localization into the rostral compartment. Our model therefore provides a new concept that indicates that a progressive oscillating wave of Notch activity is translated into the R-C polarity of a somite through the regulation of the Mesp2 expression pattern.

Anterior PSM-specific *Lfng* cannot rescue the defects in *Mesp2*-null or *Lfng*-null mice

Finally, to further ask the significance of the anterior striped cNICD domain for somite boundary formation, we established a mouse line that reproduces this expression pattern by introducing *Lfng* cDNA at the *Mesp2* locus using embryonic stem cell-mediated homologous recombination (see Fig. S1E in the supplementary material). The resulting heterozygous mice showed no abnormalities and we generated an intercross of $Mesp2^{Lfng/+}$ to yield $Mesp2^{Lfng/Lfng}$. In the $Mesp2^{Lfng/Lfng}$ embryos, cNICD signals were suppressed in the *Lfng*-expressing cells in the anterior PSM (Fig. 6B), as seen in the wild type (Fig. 6A). We further found that some of the cells that did not express *Lfng* maintained cNICD signals, indicating that Lfng suppresses cNICD production in a cell-autonomous manner (Fig. 6D). However, Lfng did not rescue the phenotype of the *Mesp2*-null mice (Fig. 6H-M), indicating that the function of *Lfng* downstream of *Mesp2* is not important.

We next introduced this transgene into the *Lfng*-null genetic background to generate a $Mesp2^{Lfng/+}Lfng^{-/-}$ mouse. The expression levels of *Lfng* in the *Mesp2* locus were found to be low (Fig. 6C,E; see Fig. S5C in the supplementary material), but we did observe downregulation of the cNICD signal in the *Mesp2*-expressing cells (Fig. 6F) in comparison with the *Lfng*-null embryos (Fig. 6G). Furthermore, *Hes5* expression (see Fig. S5D in the supplementary material), a target gene of Notch signaling, was severely downregulated in both the $Mesp2^{Lfng/Lfng}$ and $Mesp2^{Lfng/-}Lfng^{-/-}$ embryos (see Fig. S5F,H in the supplementary material) compared with *Mesp2*- and *Lfng*-null embryos (see Fig. S5E,G in the supplementary material), indicating that *Lfng* under the control of *Mesp2* might effectively suppress Notch signaling. However, we did

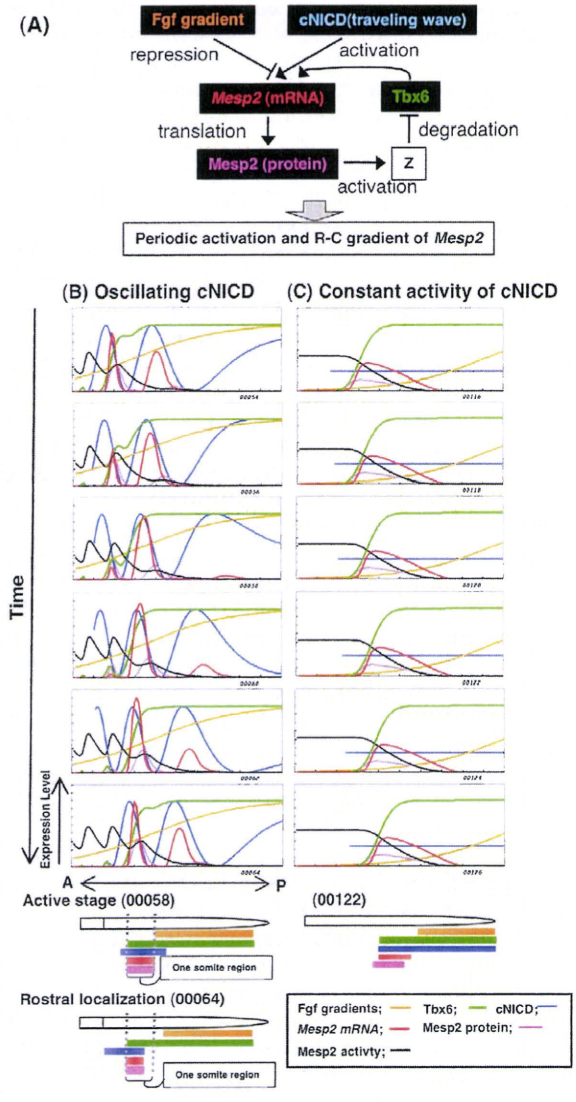

Fig. 5. Model of *Mesp2* expression. (**A**) Schematic representation indicating relationships among *Mesp2* mRNA, Mesp2 protein, Tbx6, cNICD and Fgf signaling, which is used for computer simulation to reproduce the periodic activation and R-C gradient of *Mesp2* expression. z is a hypothetical molecule that functions downstream of Mesp2 and mediates negative-feedback regulation of Tbx6. (**B**,**C**) Expression patterns of *Mesp2*, cNICD and other proteins along the anteroposterior axis predicted in our numerical model. Snapshot images of computer simulations of one cycle of somite formation in the presence (B) or absence (C) of cNICD oscillation are shown. Colored lines indicate levels of cNICD (blue), Fgf8 (orange), *Mesp2* expression (mRNA, red line; protein, pink line) and Tbx6 (green). Mesp2 activity, reflecting the total accumulation of Mesp2 protein, is shown as a tracking line in black. Data sets were taken from Movies 1 (frame 54-64) and 2 (frame 116-126) in the supplementary material, respectively. cNICD (blue) was made to disappear in the panels after one somite is formed, according to experimental observations (Morimoto et al., 2005; Oginuma et al., 2008). Lower diagrams indicate the relationships among these factors at critical time points. Snapshot (00058) corresponds to the transcriptionally active stage of *Mesp2* in which a cNICD wave (blue) reaches the anterior PSM and *Mesp2* (red) is activated in the one-somite region. Snapshot (00064) corresponds to the rostral localization stage, i.e. following the anterior shift of the cNICD wave, the *Mesp2* expression domain also shifts to the rostral region, generating a gradient of Mesp2 activity (black). As the level of cNICD is constant in the *Lfng*-null situation [corresponding to snapshot (00112)], *Mesp2* expression (red) does not show a dynamic pattern and regresses posteriorly.

not detect any significant rescue of the segmental morphology in the developing embryos or of the vertebral morphology at any level along the anteroposterior axis in the $Mesp2^{Lfng/+}Lfng^{-/-}$ mice compared with the *Lfng*-null mouse (Fig. 6N-Q; see Fig. S6 in the supplementary material). These results further confirmed that the suppression of cNICD signaling by stabilized Lfng is not sufficient for normal somitogenesis to occur.

DISCUSSION

The requirement for Notch signaling during mouse somitogenesis

In our current study, we reveal that the cNICD on/off state is not required for somite boundary formation during somitogenesis in the mouse. Consistent with this, recent studies in zebrafish embryos suggest that the function of Notch signaling is only to synchronize the oscillations among PSM cells, and that this pathway has no other function during segmentation (Riedel-Kruse et al., 2007; Horikawa et al., 2006; Ozbudak and Lewis, 2008). However, we propose from our current data that Notch signaling has a crucial function also as an output of the segmentation clock during mouse development.

This contention is supported by earlier evidence that *Mesp2* expression is severely downregulated in the absence of Notch signaling (Barrantes et al., 1999; Takahashi et al., 2000). Moreover, it has been shown that constitutive activation of Notch signaling in the paraxial mesoderm induces *Mesp2* transcription without clear on/off cycles (Feller et al., 2008) and it is also evident from other reports that Notch signaling is crucial for the establishment of R-C patterning of somites in the mouse (Takahashi et al., 2000; Takahashi et al., 2003; Feller et al., 2008). These results together suggest that the function of Notch signaling is not only to synchronize oscillations but that Notch acts also as an important output signal of the segmentation clock, at least in mouse somitogenesis. We thus speculate that Notch signaling is a key factor that mediates the transduction of clock activities into the morphological segmental pattern by regulating *Mesp2* expression. However, it is known that several oscillating components in Notch, Wnt and Fgf signaling pathways are coordinated to generate the segmentation clock network in mice. Hence, *Mesp2* transcription might not be regulated by Notch signaling alone and several pathways might govern the spatiotemporal pattern of *Mesp2* expression. The coordination of these complex networks might well be fundamental to normal somitogenesis.

A new model for the establishment of R-C polarity during somitogenesis

Based on our present findings, we propose a new function for oscillating Notch signaling, which is translated into the R-C polarity of a somite via the regulation of *Mesp2* expression in the anterior PSM. Previous models have proposed that the establishment of R-C polarity requires cell-cell communication (Takahashi et al., 2003; Dale and Pourquie, 2000), whereas we propose a model in which a

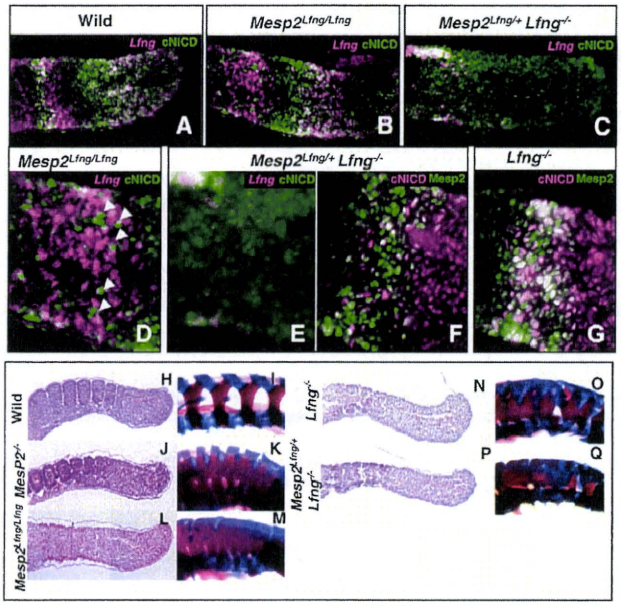

Fig. 6. Exogenous *Lfng* under the control of the *Mesp2* promoter does not rescue the phenotype of the *Mesp2*$^{-/-}$ or *Lfng*$^{-/-}$ mouse. (**A-G**) Sections of E11.5 embryos double stained for *Lfng* mRNA and cNICD (A-E) or for Mesp2 and cNICD (F,G). Higher magnification images of B and C are shown in D and E, respectively. In the *Mesp2*$^{Lfng/Lfng}$ embryo, cNICD formation (B,D, *n*=3) is suppressed in the anterior PSM. The arrowheads in D indicate *Lfng* non-expressing cells that maintain cNICD formation cell-autonomously. In the *Mesp2*$^{Lfng/+}$*Lfng*$^{-/-}$ embryos, cNICD (F, *n*=5) is effectively suppressed in the Mesp2-expressing cells compared with *Lfng*-null embryos (G, *n*=6). (**H-Q**) Comparison of the segmental morphologies in the E11.5 embryonic tail region (H,J,L,N,P) and E17.5 vertebral region (I,K,M,O,Q) among the different genotypes indicated. Neither the *Mesp2*$^{Lfng/Lfng}$ (L,M) nor *Mesp2*$^{Lfng/+}$*Lfng*$^{-/-}$ (P,Q) mice show any recovery of the *Mesp2*$^{-/-}$ (J,K) or *Lfng*$^{-/-}$ (N,O) phenotypes. Number of samples: H, *n*=4; I, *n*=6; J, *n*=3; K, *n*=4; L, *n*=3; M, *n*=6; N, *n*=3; O, *n*=6; P, *n*=3; Q, *n*=7.

cell-autonomous mechanism utilizes Notch signaling oscillation in the posterior PSM. This notion is further supported by computer simulations, in which we found that an appropriate translation of spatiotemporal information provided by the traveling wave of cNICD is sufficient to create the dynamic *Mesp2* expression pattern, i.e. on/off cycles and rostral localization (Fig. 5B; see Movie 1 in the supplementary material). In these simulation experiments, the generation of the traveling wave was based on the earlier work of Lewis (Palmeirim et al., 1997), and the translation of the wave information into *Mesp2* expression was modeled on the gene network that we elucidated previously (Oginuma et al., 2008; Yasuhiko et al., 2006). In the model, the cNICD wave, an activator of *Mesp2*, travels from the posterior to the anterior, whereas the levels of Fgf, a repressor of *Mesp2*, are higher toward the posterior. Consequently, as a single wave passes through a nascent somite, the net transcriptional activation of *Mesp2*, which reflects the amount of cNICD subtracted by the amount of Fgf, is higher toward the rostral part of the presumptive somite. The resulting gradient of Mesp2 activity might thus allow PSM cells to establish a rostral identity and the segmental border. Hence, this is the first model to demonstrate that R-C polarity in the somite is generated as a direct output of the segmentation clock.

The repression of Tbx6, an activator of *Mesp2*, downstream of Mesp2 is another important component in our model. This regulatory module prevents *Mesp2* expression after one traveling wave of cNICD has passed, and thus fixes the R-C gradient pattern of Mesp2. The next wave of Notch signaling cannot affect the Mesp2 pattern created by the former wave. To reproduce the intensive degradation of Tbx6 at anterior regions, we had to adjust the parameters for Tbx6 degradation. We did not need to change any of the other standard parameters we initially chose, suggesting that the qualitative features of the model are not so sensitive to the quantitative values of the parameters. In our simulation analysis, however, we did not reproduce the sharp anterior boundaries of Tbx6 and Mesp2 accumulation (green and black lines, respectively, in Fig. 5B; see Movie 1 in the supplementary material) that have been observed in vivo. To create a sharp boundary of Tbx6 and Mesp2, which should be required to create a fine segmentation boundary, further adjustment of the parameters or another mechanism might be required. In this regard, the next important challenge will be to investigate the molecular basis of the sharpening expression boundaries of Tbx6 and Mesp2, and ultimately to understand how analog inputs (such as sequential wave patterns of oscillation) are converted into digital outputs (such as the square-like stair patterns of the segmental border).

Functions of Lfng in the posterior and anterior PSM during mouse somitogenesis

We also demonstrate from our present data that the oscillatory expression of *Lfng* is both required and sufficient for normal somitogenesis. However, this result will probably be viewed somewhat controversially given the recent findings that have underscored the significance of Lfng expression in the anterior PSM during this process, at least after E10.5 (Shifley et al., 2008; Stauber et al., 2009). The authors of these reports produced transgenic mice harboring *Lfng* expression without oscillation. Their data indicate that cNICD oscillation is disrupted, but that normal segmented somites form, after E10.5 and they concluded that oscillating *Lfng* expression is required only for early stage, but not later stage, somitogenesis (Shifley et al., 2008; Stauber et al., 2009). We wish therefore to discuss some possible explanations for the discrepancies between our current findings and these previous experimental results.

One possibility is that the common expression profiles between our *Hes7>Lfng* mouse and the mice studied in previous reports is important. We demonstrate here that *Hes7* and *Lfng* expression manifest a waved pattern within the Tbx6 expression domain, which includes a part of the anterior PSM. Therefore, in our *Hes7>Lfng* mouse, oscillating *Lfng* expression also exists in the anterior PSM, but not as a stabilized pattern. We suspect that the transgenic mice analyzed in previous reports lack oscillating *Lfng* expression in the posterior PSM but the oscillation might exist in the anterior PSM as well, and thus we speculate that the oscillating *Lfng* expression in the posterior PSM is not required after E10.5, but that in the anterior PSM might be sufficient for normal somitogenesis. Another possibility is that the slightly oscillating expression reported previously might be responsible for the rescue event. Previous studies have shown that two distinct enhancers are involved in the oscillatory expression of *Lfng*, one of which is disrupted in the mouse reported by Shifley et al. (Shifley et al., 2008), and a slight cyclic expression of *Lfng* exists in the mouse generated by Stauber et al. (Stauber et al., 2009). Hence, one possible interpretation for these discrepancies is that the slight cyclic expression of *Lfng* might be sufficient for normal development in the enhancer-specific